Numerička simulacija procesa spreja i izgaranja u komori za izgaranje mlaznog motora

Cerinski, Damijan

UNIVERSITY OF ZAGREB
FACULTY OF MECHANICAL ENGINEERING AND NAVAL ARCHITECTURE

MASTER'S THESIS

Damijan Cerinski

Zagreb, 2017.

UNIVERSITY OF ZAGREB
FACULTY OF MECHANICAL ENGINEERING AND NAVAL ARCHITECTURE

MASTER'S THESIS

Supervisor:

Asst. prof. dr. sc. Milan Vujanović

Student:

Damijan Cerinski

Zagreb, 2017.

I hereby declare that this thesis is entirely the result of my own work except where otherwise indicated. I have fully cited all used sources, and I have only used the ones given in the list of references.

I am genuinely thankful to Associate Professor Milan Vujanović, for giving me an opportunity to work in his group and being the supervisor of the thesis.

Special thanks for project assistant Dr. Zvonimir Petranović, for everyday unselfish support, guidance and opportunity to learn. His knowledge, insights, help and advice significantly contributed to the quality of work presented in this thesis.

I would like to express my gratitude to Masoud Hajivand for providing the geometry of the radial swirler.

I would also like to acknowledge the financial support of Adria Section of the Combustion Institute (ASCI).

I need to thank my colleagues from the PowerLab CFD office, who also helped me a lot through this thesis and created great working environment every day: Dr. Jakov Baleta, Dr. Hrvoje Mikulčić, Dr. Marko Ban, Tibor Bešenić and Filip Jurić.

Also, I would like to thank my family and friends for believing in me without a doubt, and supporting me through my whole education.

Finally, greatest thanks to my girlfriend, Vanesa. She is always there, beside me, when I need her the most.

Damijan Cerinski

SVEUČILIŠTE U ZAGREBU
FAKULTET STROJARSTVA I BRODOGRADNJE
Središnje povjerenstvo za završne i diplomske ispite
Povjerenstvo za završne i diplomske ispite studija zrakoplovstva

Sveučilište u Zagrebu Fakultet strojarstva i brodogradnje	
Datum	Prilog
Klasa:	
Ur.broj:	

DIPLOMSKI ZADATAK

Student: **Damijan Cerinski** Mat. br.: 0035186073

Naslov rada na hrvatskom jeziku: **Numerička simulacija procesa spreja i izgaranja u komori za izgaranje mlaznog motora**

Naslov rada na engleskom jeziku: **Numerical Modelling of Spray and Combustion Processes in a Jet Engine Combustion Chamber**

Opis zadatka:

Korištenje računalne dinamike fluida (RDF) u kombinaciji s eksperimentalnim pristupom postao je uobičajen pristup u razvoju različitih inženjerskih sustava. Uslijed utjecaja inercije, površinske napetosti i aerodinamičkih sila dolazi do raspadanja goriva na sitne kapljice, njihovog isparavanja te miješanja sa smjesom plinova. Prilikom rada mlaznog motora, unutar komore za izgaranje dolazi do stvaranja spreja i miješanja goriva sa zrakom te do procesa zapaljenja. U okviru diplomskog zadatka potrebno je:

1. Opisati osnovne jednadžbe računalne dinamike fluida te opisati jednadžbe korištene za opisivanje procesa spreja i procesa izgaranja;
2. Prikazati numeričke postavke koje će se koristiti za riješavanje problema;
3. Računalno modelirati proces ubrizgavanja i proces izgaranja u komori mlaznog motora;
4. Obrazložiti izračunate rezultate kao što su profili temperature i koncentracije kemijskih vrsta. Nadalje, analizirati utjecaj spreja na distribuciju isparenog goriva i profile temperatura. Sva potrebna literatura, opis modela te ulazni i početni podaci za analizu slučaja bit će dostupni od strane mentora i neposrednog voditelja.

U radu je potrebno navesti korištenu literaturu i eventualno dobivenu pomoć.

Zadatak zadan:	Rok predaje rada:	Predviđeni datumi obrane:
11. svibnja 2017.	13. srpnja 2017.	19., 20. i 21. srpnja 2017.

Zadatak zadao: Predsjednik Povjerenstva:

Doc. dr. sc. Milan Vujanović Prof. dr. sc. Ivica Smojver

LIST OF CONTENT

LIST OF FIGURES

LIST OF TABLES

NOMENCLATURE

Latin	**Unit**	**Description**
u	m/s	Velocity
S	m^2	Surface
V	m^3	Volume
t	s	Time
x_i	m	Cartesian coordinates
e	J/kg	Specific energy
T	K	Temperature
Y	-	Mass fraction
m	kg	Mass
D_k	m^2/s	Diffusion coefficient
S	-	Source
A	-	Constant in Arrhenius law
c	kg/m^3	Concentration
C	-	Model coefficient
E_a	J/kg	Activation energy
k	m^2/s^2	Turbulent kinetic energy
f	-	Fuel mass fraction
g	-	Mass fraction of gas residuals
F_d	N	Drag force
p	Pa	Pressure
q	W/kg	Specific heat
T	s	Turbulent time scale
L	m	Turbulent length scale

Greek	**Unit**	**Description**
β	-	Coefficient in Arrhenius law
Γ	-	Diffusion coefficient
δ_{ij}	-	Kronecker delta
λ	$W/(mK)^{-1}$	Thermal conductivity coefficient

ε	m	Turbulent kinetic dissipation rate
λ_w	m	Wavelength
μ	Pas	Dynamic viscosity
μ_t	Pas	Turbulent viscosity
ρ	kg/m^3	Density
σ	N/m	Surface tension
σ_{ji}	N/m^2	Stress tensor
τ	N/m^2	Viscous stress
τ_a	s	Breakup time
υ	m^2/s	Kinetic viscosity
φ	-	Extensive property
ω	-	Combustion source
Ω	s	Wave growth rate

Dimensionless	***quantity***
Nu	Nusselt number
Pr	Prandtl number
Re	Reynolds number
Oh	Ohnesorge number
We	Weber number
Sh	Sherwood number

ABSTRACT

In this thesis, numerical modelling of combustion process in a can type combustion chamber of a jet engine is presented. The observed chamber is designed with a double stage radial swirler used to induce air vortices. The constant mass flow air is defined at the combustion chamber inlet in order to supply the combustion zone with fresh oxygen. The liquid fuel Jet-A was used as a surrogate for the kerosene fuel. To model the turbulent behaviour, the advanced $k-\zeta-f$ turbulence model was utilised, whilst the spray process was described by using the Euler Lagrangian approach. The combustion process was described with the ECFM-3Z combustion model, and the ignition was modelled with the Imposed stretch spark ignition model. The influence of droplet spreading angle on the combustion process was analysed. Presented results, such as temperature distribution, velocity profiles, and emission concentrations through the entire combustion chamber were verified. According to the provided results, a correct chemical and physical behaviour of the chosen setup was achieved. All simulations were performed with the commercial computational fluid dynamic software AVL FIRE™.

Key words: CFD, modelling, combustion, Jet engine, kerosene

SAŽETAK

U ovom radu, izvršeno je numeričko modeliranje procesa spreja i izgaranja unutar komore za izgaranje mlaznog motora. Promatrana komora sastoji se od dvostupanjskog radijalnog vrtložnika koji se koristi za induciranje vrtloga zraka. Na ulazu u komoru propisan je konstantan protok zraka kako bi se osiguralo dovoljno kisika u zoni izgaranja. U ovom radu tekuće gorivo Jet-A korišteno je kao zamjena za kerozin. Za modeliranje turbulentnog strujanja korišten je napredni $k-\zeta-f$ model turbulencije, dok je za opisivanje procesa spreja korišten Euler Lagrangeov pristup modeliranja spreja. Proces izgaranja modeliran je pomoću ECFM-3Z modela izgaranja dok je proces zapaljenja modeliran korištenjem ISSIM modela zapaljenja. Utjecaj spreja analiziran je provođenjem simulacija s različitim kutom spreja. Verificirani su prezentirani rezultati, kao što su temperaturna raspodjela, profili brzine te koncentracija emisija kroz komoru za izgaranje. S obzirom na dobivene rezultate, može se zaključiti da je postignuto ispravno fizikalno i kemijsko ponašanje unutar komore izgaranja. Sve simulacije su odrađene u komercijalnom RDF programu AVL FIRE™.

Ključne riječi: RDF, modeliranje, izgaranje, mlazni motor, kerozin

PROŠIRENI SAŽETAK

(EXTENDED ABSTRACT IN CROATIAN)

UVOD

Mlazni motori su danas široko korišteni u komercijalnom zrakoplovstvu zbog visokog omjera potisne sile i težine te njihove pouzdanosti. Efikasnost mlaznih motora je niža u usporedbi s klipnim motorima, što uzrokuje višu specifičnu potrošnju goriva. Jedan način povećanja efikasnosti je optimiziranje procesa izgaranja. Cilj ovog rada je istražiti karakteristike procesa izgaranja u komorama za izgaranje mlaznog motora koristeći Računalnu Dinamiku Fluida (RDF). Korištenjem RDF moguće je detaljno analizirati različite procese te dobiti uvid u rezultate kao što su: temperaturna polja, koncentracije isparenog goriva i štetnih emisija, polja brzina i slično. Rezultati dobiveni RDF mogu se implementirati na realne konstrukcije komora za izgaranje u svrhu njihova poboljšanja. Proces spreja goriva ima znatan utjecaj na efikasnost procesa izgaranja te se iz tog razloga moraju koristiti odgovarajući modeli koji će opisati fizikalno i kemijsko ponašanje spreja. U ovom radu za modeliranje procesa spreja korišten je Euler Lagrangeov pristup, dok je proces izgaranja je modeliran naprednim ECFM-3Z modelom izgaranja u kombinaciji s ISSIM pristupom modeliranja zapaljenja smjese.

MATEMATIČKI MODEL

U ovom odlomku opisani su matematički modeli korišteni za modeliranje procesa spreja, izgaranja, turbulencije, formiranja emisija te prijenosa kemijskih vrsta. Glavna pretpostavka matematičkog modela je da se plinovita faza unutar komore za izgaranje smatra kontinuumom te se za nju rješavanju transportne jednadžbe očuvanja (Eulerov pristup). Opća transportna jednadžba se može izraziti kao:

$$\underbrace{\int_V \frac{\partial}{\partial t}(\rho\varphi)dV}_{nestacionarni\ član} + \underbrace{\int_S (\rho\varphi)\, u_i\, n_i\, dS}_{konvekcija} = \underbrace{\int_S \left(\Gamma_\varphi \frac{\partial \varphi}{\partial x_i}\right) n_i\, dS}_{difuzija} + \underbrace{\int_V S_\varphi\, dV}_{izvor/ponor}. \qquad (1.1)$$

Zamjenom oznake φ s nekom fizikalnom veličinom dobivaju se izrazi za određene zakone očuvanja fizikalnog svojstva. Zamjenom člana s gustoćom, ρ dobiva se zakon očuvanja mase,

zamjenom s ρu_i zakon očuvanja količine gibanja, zamjenom s ρe zakon očuvanja energije te zamjenom s y_k zakon očuvanja mase kemijske vrste k.

Modeliranje turbulencije

Turbulentno strujanje je specifično za gotovo sve inženjerske sustave te se iz tog razloga koriste modeli turbulencije koji ubrzavaju vrijeme računanja aproksimirajući stvarno strujanje osrednjenim veličinama. U ovom radu korišten je napredni $k-\zeta-f$ model turbulencije koji rješava 4 transportne jednadžbe. Taj model je odabran zbog svoje robusnosti za modeliranje strujanja gdje postoji značajno skretanje toka fluida, što je karakteristično za promatrani inženjerski problem.

Modeliranje spreja

U ovom radu korišten je Euler Lagrangeov pristup modeliranja procesa spreja. Takav pristup tekuće gorivo sortira u grupu kapljica sličnih promjera i fizikalnih svojstava, referenciranih kao parcele. Za svaku parcelu, računaju se njihove trajektorije dok se za plinovitu fazu rješavaju jednadžbe očuvanja mase, količine gibanja i energije. Gorivo je ubrizgano u komoru za izgaranje kroz sapnicu malog promjera te je izloženo aerodinamičkim i turbulentnim silama koje uzrokuju raspadanje kapljica. Jednadžba očuvanja količine gibanja spreja opisana je promjenom količine gibanja kapljice u vremenu koja je jednaka sili otpora koja djeluje na kapljicu:

$$m_p \frac{du_{ip}}{dt} = F_{idr}. \tag{1.2}$$

U jednadžbi (1.2) m_p označava masu parcele dok je F_{idr} sila otpora. Unutar procesa spreja korištena su dva različita fizikalna modela. Za modeliranje procesa raspadanja kapljica korišten je WAVE model, dok je Abramzon-Sirignano model korišten za modeliranje isparavanja kapljica.

<u>WAVE model raspadanja</u>

U ovom radu , WAVE model je korišten za modeliranje raspadanja kapljica. Izražena relativna brzina između kapljice goriva i struje zraka rezultira nastajanjem nestabilnih površinskih

valova. Zbog rasta tih valova dolazi do odvajanja mase i kreiranja novih kapljica manjeg promjera. Veza između radijusa novo nastale kapljice, r_{stable} i valne duljine najbrže rastućeg vala, Λ dana je jednadžbom:

$$r_{stable} = C_1\Lambda. \tag{1.3}$$

U jednadžbi (1.3) izraz C_1 je konstanta modela te je njena vrijednost postavljena na preporučenu vrijednost prema literaturi, 0.61. Vrijeme potrebno za proces raspadanja, τ_a određeno je formulom:

$$\tau_a = \frac{3.726 C_2 r_k}{\Lambda_k \Omega_k}, \tag{1.4}$$

gdje izraz r_k označava radijus matične kapljice, Ω_k je vrijednost brzine rasta vala, a Λ_k je valna duljina. Konstanta modela C_2 služi za korekciju vremena potrebnog za proces raspadanja. Preporučene vrijednosti te konstante kreću se između 1.73 i 160 gdje niže vrijednosti rezultiraju intenzivnijim procesom raspadanja.

Abramzon-Sirignano model isparavanja

Nakon procesa raspadanja, kapljice isparavaju uslijed visoke temperature unutar komore za izgaranje. Za modeliranje procesa isparavanja korišten je Abramzon-Sirignano model. Specifično za taj model je pretpostavka jednolike raspodjele temperature po promjeru kapljice te njezina sferična geometrija.

Modeliranje izgaranja

U ovom radu, napredni ECFM-3Z model je korišten za modeliranje izgaranja. Unutar tog modela rješavaju se transportne jednadžbe za masene udjele kemijskih vrsta kao što su: gorivo, O_2, N_2, NO, CO_2, CO, H_2, H_2O, O, H, N i OH unutar 3 zone miješanja. Taj model izgaranja može biti korišten s modelom za opisivanje zapaljenja smjese.

Modeliranje štetnih emisija

U ovom radu za modeliranje štetnih emisija korišten je prošireni Zeldovich model pomoću kojeg se modelira stvaranje termalnog NO_x-a. Za točnije opisivanje koncentracije štetnih emisija, uzeto je u obzir i stvaranje promptnog NO_x-a.

Standardni transportni model kemijskih vrsta

Prijenos kemijskih vrsta modeliran je standardnim modelom koji rješava tri transportne jednadžbe:

- Maseni udio neizgorenog goriva, y_{fu};
- Maseni udio goriva, f;
- Maseni udio zaostalih produkata plinova, g;

NUMERIČKE POSTAVKE

Numeričke simulacije odrađene su u komercijalnom programskom paketu AVL FIRE™. U ovom poglavlju prvo će biti prikazane numeričke postavke simulacija za provjeru utjecaja mreže te će nakon toga biti pokazane postavke korištene za modeliranje procesa spreja.

Postavke računalnih simulacija za provjeru utjecaja mreže

Test utjecaja mreže je izvršen za tri računalne mreže s različitim brojem kontrolnih volumena. Mreže nazvane *gruba*, *fina* i *finija* generirane su s 336042, 460415 i 701823 kontrolnih volumena te su na slici 1 prikazani njihovi presjeci u blizini vrtložnika.

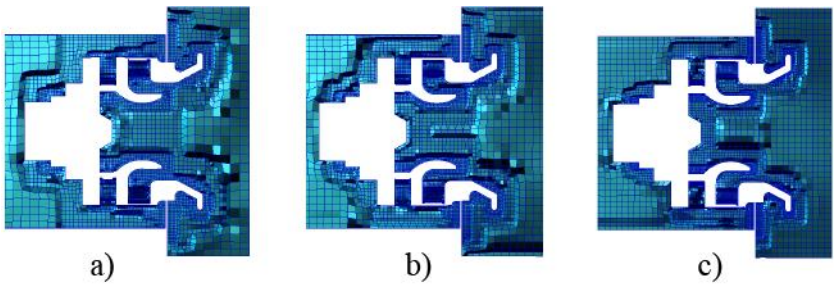

Slika 1 Distribucija kontrolnih volumena oko vrtložnika a) gruba, b) fina, c) finija

Početni i rubni uvjeti

Selekcije koje su korištene za rubne uvjete na gruboj mreži su prikazane na slici 2 te se za ostale mreže koristila ista konfiguracija. Na ulaznim selekcijama zraka i goriva propisani su konstantni maseni protoci s konstantnim temperaturama. Na izlaznoj selekciji postavljen je konstantan statički tlak te su za sve zidove propisani adijabatski rubni uvjeti. Kod izvođenja testa utjecaja mreže, temperatura svih zidova postavljena je na 293.15 K i proces spreja nije se uzimao u obzir. Vrijednosti rubnih uvjeta prikazani su u tablici 1, dok su korišteni početni uvjeti prikazani u tablici 2.

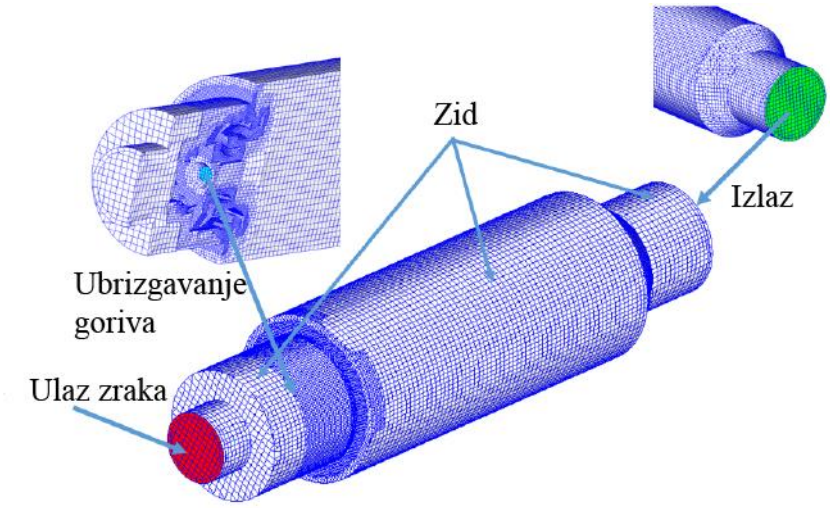

Slika 2 Selekcije za rubne uvjete

Tablica 1 Rubni uvjeti

Maseni protok zraka	0.8 kg/s
Temperatura zraka	650 K
Maseni protok goriva	0.023 kg/s
Temperatura goriva	300 K
Zid	Adijabatski rubni uvjeti
Tlak na izlazu	9.12 bar

Tablica 2 Početni uvjeti

Tlak	9.12 bar
Temperatura	650 K
Turbulentna skala duljine	0.001 m
Turbulentna kinetička energija	0.001 m^2s^{-2}
Gustoća	Jednadžba idealnog plina

Postavke procesa spreja

Shematski prikaz sapnice prikazan je na slici 3. Promjer kapljica goriva na izlazu iz sapnice iznosi $150\ \mu m$. Izračunate su tri različite simulacije s različitim kutom spreja koji je određen pomoću kutova δ_1 i δ_2. δ_1 označava polovicu kuta vanjskog konusa, a δ_2 polovicu kuta unutrašnjeg konusa. U tablici 3 prikazane su tri promatrane konfiguracije sapnice.

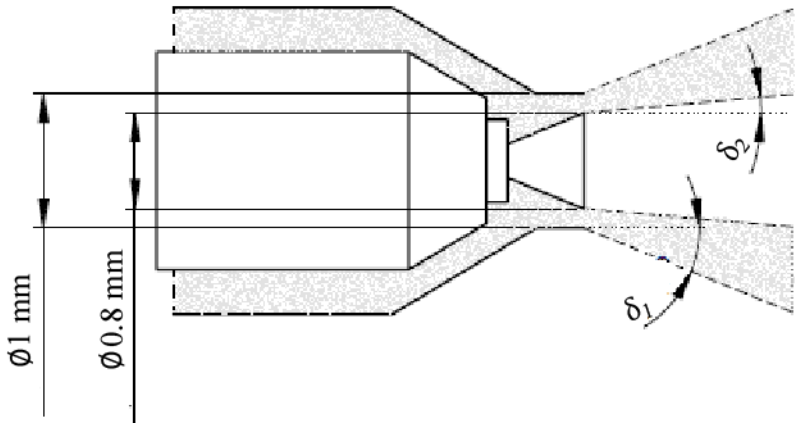

Slika 3 Shematski prikaz sapnice

Tablica 3 Konfiguracije sapnice

Kut spreja [°]	$\boldsymbol{\delta_1}$ [°]	$\boldsymbol{\delta_2}$ [°]
15	18	3
20	22	2
25	28	3

REZULTATI

Rezultati koji će biti prikazani su polja temperature i brzine, distribucije dušičnih oksida te procesi spreja i isparenog goriva kroz komoru za izgaranje. Prvo će biti prikazani rezultati testa utjecaja mreže. Nakon toga analizirat će se utjecaj konfiguracije sapnice na proces izgaranja, dok će se na kraju rada prikazati rezultati za kvazistacionarno razvijeno stanje.

Test utjecaja mreže

Rezultati koji će biti promatrani su polja brzine i temperature u računalnoj domeni oko vrtložnika za tri različite konfiguracije mreže.

Na slici 4 prikazani su rezultati polja brzine i temperature zraka za vremenski trenutak 2 ms. U tom vremenskom trenutku, postignuto je kvazistacionarno strujanje. Prikazani rezultati se podudaraju za sve tri računalne mreže, uz malo odstupanje u raspodjeli temperature uspoređujući grubu i finiju mrežu. Na istoj slici može se vidjeti ubrzanje struje zraka prolaskom kroz vrtložnik te generiranje vrtloga na izlazu iz vrtložnika.

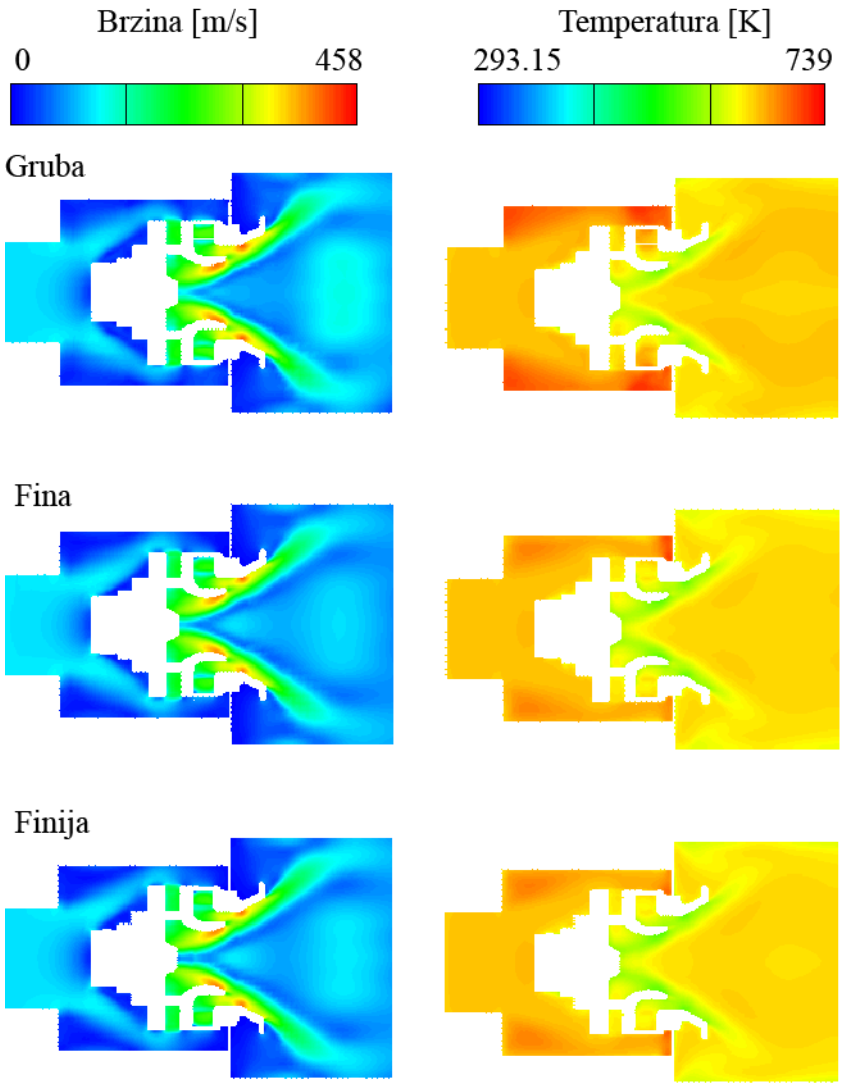

Slika 4 Polja brzine i temperature za vremenski trenutak 2 ms

Na slici 5 prikazana su polja brzine i temperature zraka na presjeku u smjeru *x* osi na udaljenosti 0.1 m od selekcije ulaza zraka. Može se primijetiti da je nakon vrtložnika postignuto jednoliko strujanje za sve tri promatrane računalne mreže.

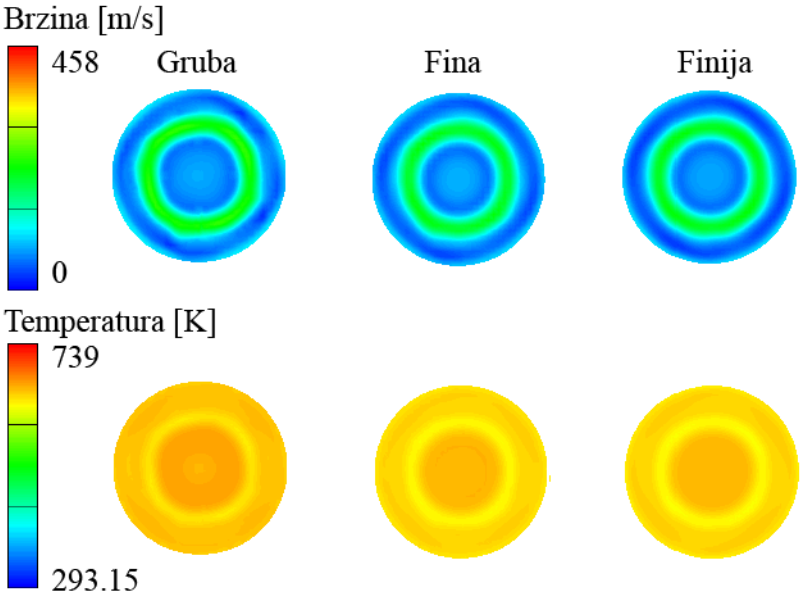

Slika 5 Polja brzine i temperature u presjeku *x* osi

Test utjecaja mreže pokazuje da tijekom strujanja zraka kroz radijalni vrtložnik te nakon postignutog kvazistacionarnog strujanja rezultati polja brzine i temperature su slični za sve tri računalne mreže. Kako postoji malo odstupanje u temperaturi između grube i fine mreže, gruba mreža je korištena za sve daljnje računalne simulacije. Smatra se da će odabrana mreža dati zadovoljavajuće rezultate za potrebe ovog rada.

Kvazistacionarno stanje

Kvazistacionarno stanje je postignuto kada oscilacije srednje temperature i masenog udjela NO_x-a unutar komore za izgaranje ostaju na niskim vrijednostima sa svakim novim vremenskim korakom. Na slici 6 promatrajući srednju temperaturu unutar komore, vidi se postizanje kvazistacionarnog stanja nakon 20 ms simulacije, dok je promatrajući maseni udio NO_x-a, kvazistacionarno stanje postignuto nakon 30 ms simulacije. Dijagrami na slici 6 prikazani su za simulaciju s kutom spreja od 20°, dok je za ostale simulacije kvazistacionarno stanje postignuto u sličnom vremenskom razdoblju. Daljnji rezultati, referencirani s kvazistacionarnim stanjem, prikazani su za vrijeme simulacije od 30 ms.

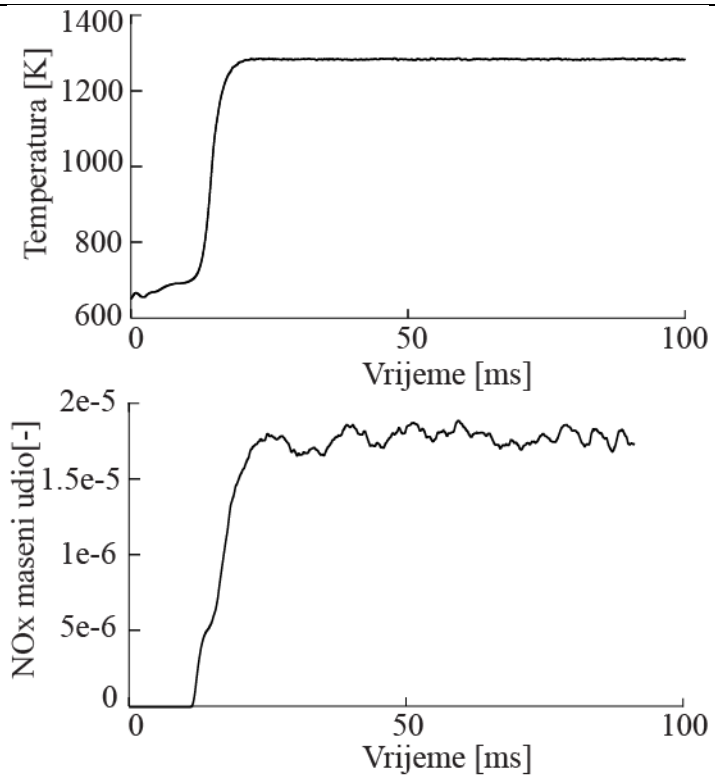

Slika 6 Srednja temperatura i maseni udio NO_x-a u komori za izgaranje

Utjecaj spreja

Ubrizgavanje goriva počinje 2 ms nakon početka računalne simulacije. Na lijevoj strani na slici 7 prikazani su oblici raspršivanja spreja za različite kutove konfiguracije sapnice. Vidljivo je da s većim kutom dolazi do intenzivnijeg raspršivanja kapljica goriva. Na desnoj strani iste slike prikazano je ispareno gorivo za različite kutove spreja. Vidljivo je da je maseni udio isparenog goriva sličan za kutove spreja 15° i 20°, dok je s kutom spreja 25° isparilo znatno manje goriva.

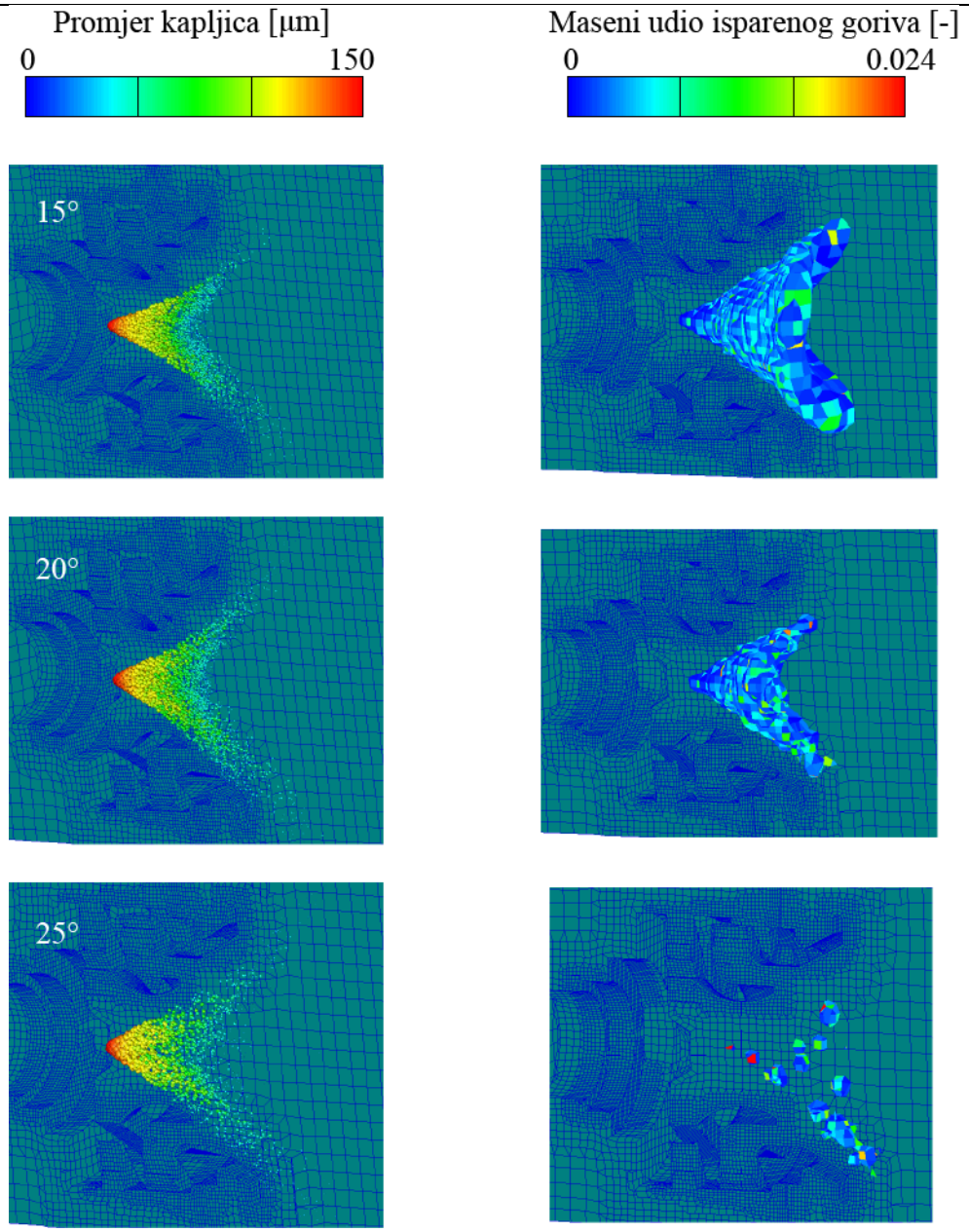

Slika 7 Distribucija kapljevitog i plinovitog goriva za različite kutove spreja

Na lijevoj strani slike 8 prikazana je temperaturna distribucija za simulacije s različitim kutovima spreja. Na slici se vidi da za simulacije s kutovima spreja od 15° i 20°, lokalna temperatura je puno viša i jednoliko raspoređena kroz komoru za izgaranje, uspoređujući sa simulacijom gdje je kut spreja 25°. Također, vidljivo je da je temperatura s kutom spreja od 20° viša od temperature s kutom spreja 15°. Na desnoj strani slike 8 distribucija NO_x-a je prikazana te se vidi da je distribucija slična za kutove spreja 15° i 20°, dok je znatno niža za simulaciju s kutom spreja 25° zbog niže temperature unutar komore za izgaranje.

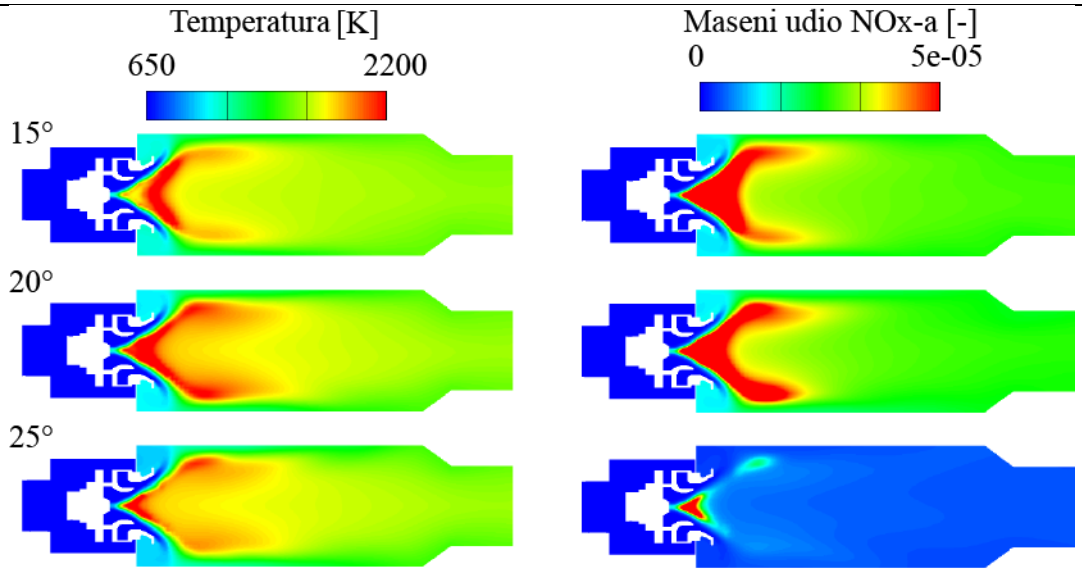

Slika 8 Temperaturna raspodjela i raspodjela NO_x-a za različite kutove spreja

Proces izgaranja

Proces izgaranja počinje otprilike nakon 15 ms od početka računalne simulacije. U ovom radu, u cilju ubrzavanja konvergencije simulacija, korišten je model s više svjećica za zapaljenje.

Na slici 9 prikazan je razvoj regija visokih temperatura unutar komore za izgaranje. Na lijevoj strani prikazana je temperaturna distribucija za četiri različita vremenska koraka, dok je na desnoj strani iste slike prikazano stvaranje emisije NO_x-a. Vidljivo je da u regijama niže temperature ne dolazi do stvaranja NO_x-a. Kada temperatura dosegne više vrijednosti, NO_x se počinje generirati te prati regije visokih temperatura.

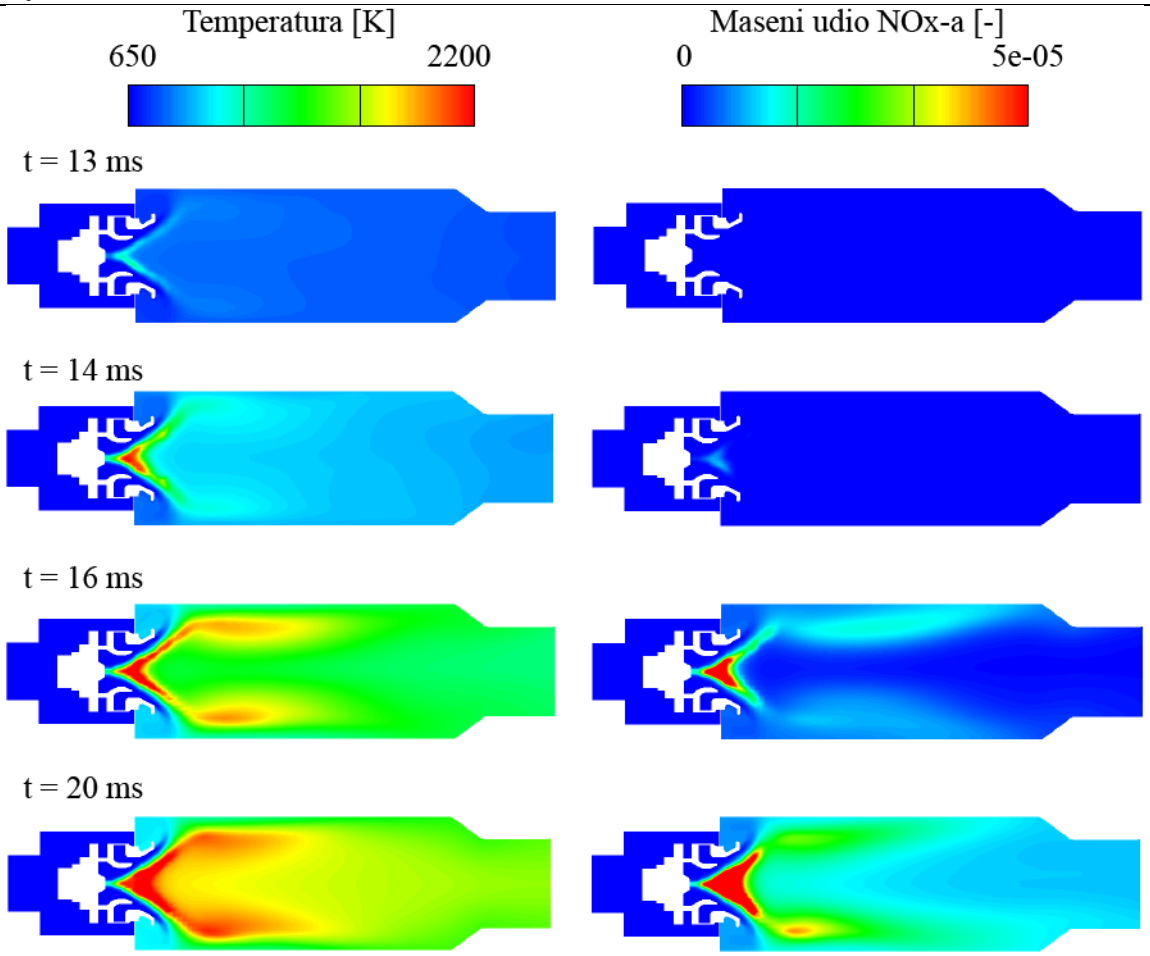

Slika 9 Temperaturna raspodjela i raspodjela NO_x-a unutar komore za izgaranje

Temperaturne raspodjele i raspodjela masenog udjela NO_x-a za poprečne presjeke na različitim udaljenostima u smjeru *x* osi prikazane su na slici 10. Prvi presjek smješten je na udaljenosti 100 *mm* od selekcije ulaza zraka te je svaki sljedeći presjek udaljen dodatnih 10 *mm* u smjeru strujanja. Iz prikazanih rezultata vidi se da je postignuto jednoliko strujanje, što je bitno zbog smanjenja gubitaka tlaka u turbinskom dijelu.

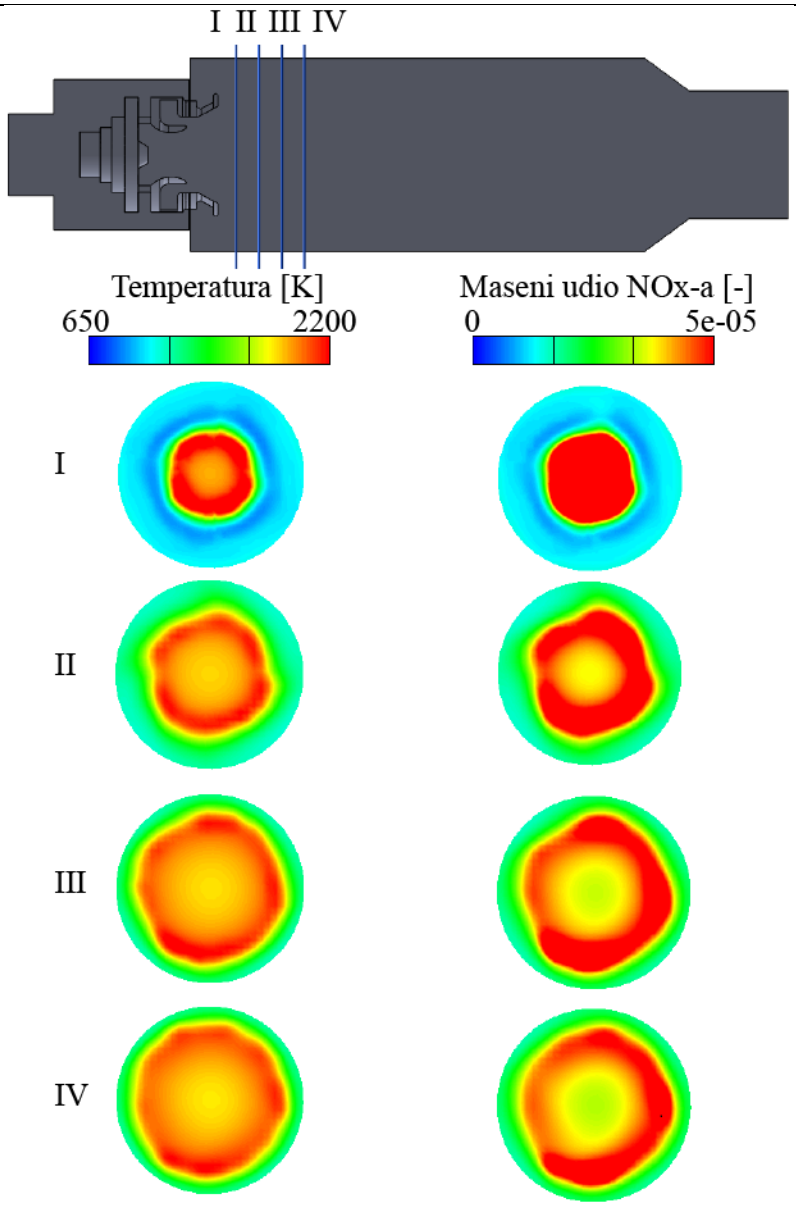

Slika 10 Temperaturna raspodjela i raspodjela NO_x-a na različitim udaljenostima u smjeru strujanja zraka

1. INTRODUCTION

Jet engines are widely used today in commercial aviation as a consequence of their great thrust to weight ratio and their reliability. The efficiency of a jet engine is lower when comparing to piston engines, which results in a much higher specific fuel consumption [1]. One way to improve the efficiency of a jet engine is to optimise the combustion process. The purpose of this study is to investigate characteristics of the combustion process in a can type combustion chamber of a jet engine by using the Computational Fluid Dynamics (CFD).

1.1. The working cycle of gas turbine engine

The working cycle of gas turbine engine is usually connected to the Brayton cycle, which is shown in the $p-v$ and $T-s$ diagram in Figure 1. The ideal Brayton cycle consists of isentropic compression (1-2), isobaric combustion (2-3), isentropic expansion (3-4) and isobaric heat release (4-1). Inside the gas turbine engine, four different processes occur: intake, compression, combustion, and exhaust process. All the mentioned processes occur in a separate part of the engine at the same time and they are shown in Figure 2. Initially, the air is entrained into the engine and it is compressed by utilising the jet engine compressor. The compressed air flows into the combustion chamber and combusts in contact with the vaporised fuel. The hot gaseous mixture of combustion products passes through the engine turbine where a certain amount of the energy required for running compressor is extracted. The mixture of expanded gases passes through the propelling nozzle creating the thrust force.

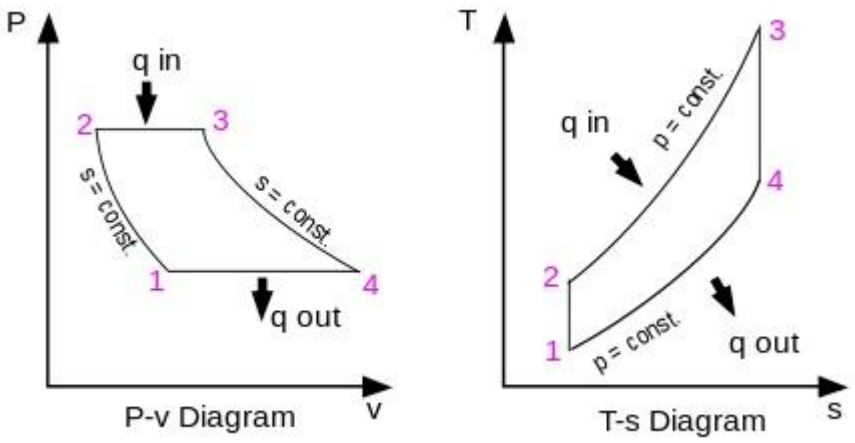

Figure 1 The ideal Brayton cycle [2]

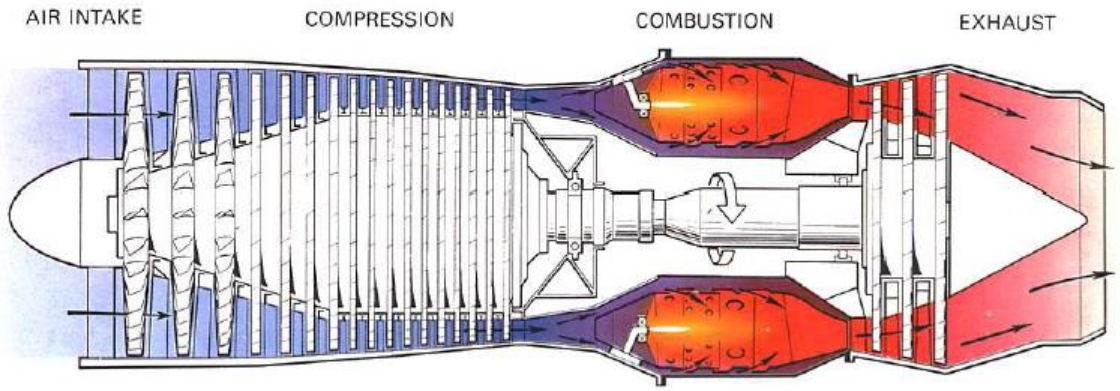

Figure 2 Schematic of processes within the jet engine [3]

1.1.1. Intake

The air with the state corresponding to the environment pressure and temperature inflow into the jet engine where several conditions must be obtained:

- Maximize return pressure – turning kinetic energy in pressure;
- Minimize drag force;
- Minimize fan and compressor noise – which is important because of strict regulations;
- Ensure flow stability independence by changing the angle of attack – to supply the compressor with uniform air flow at all flight conditions;

1.1.2. Compression

In the gas turbine engine, the compression of entrained air is effected by one of two basic types of compressor, centrifugal or radial compressor. Both types are driven by the turbine and are usually connected directly to the turbine shaft. The mentioned compressors are different in design which results in different pressure and velocity profiles, as discussed:

1. The centrifugal compressor can be a single or two stage unit employing impeller to accelerate the air and diffuser to produce required pressure rise. Pressure and velocity changes through a centrifugal compressor are shown in Figure 3.

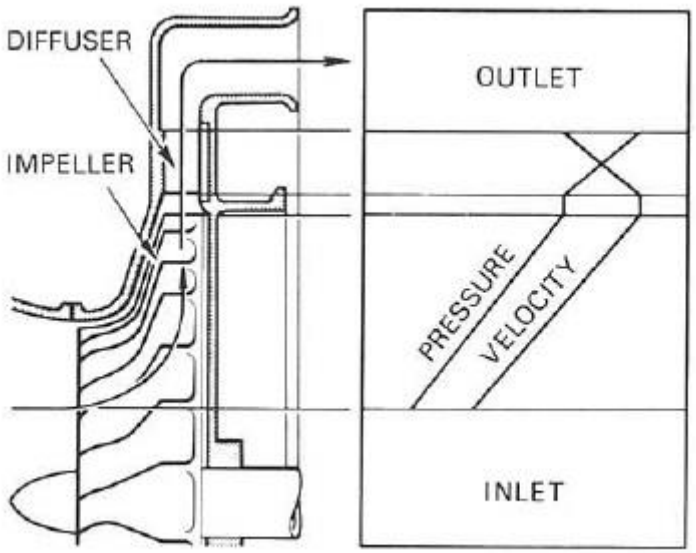

Figure 3 Pressure and velocity profiles through a centrifugal compressor [3]

2. The axial compressor is a multi-stage unit employing alternate rows of rotating (rotor) blades and stationary (stator) vanes that are used to accelerate and diffuse the air until the required pressure rise is obtained. Pressure and velocity change through an axial compressor is shown in Figure 4

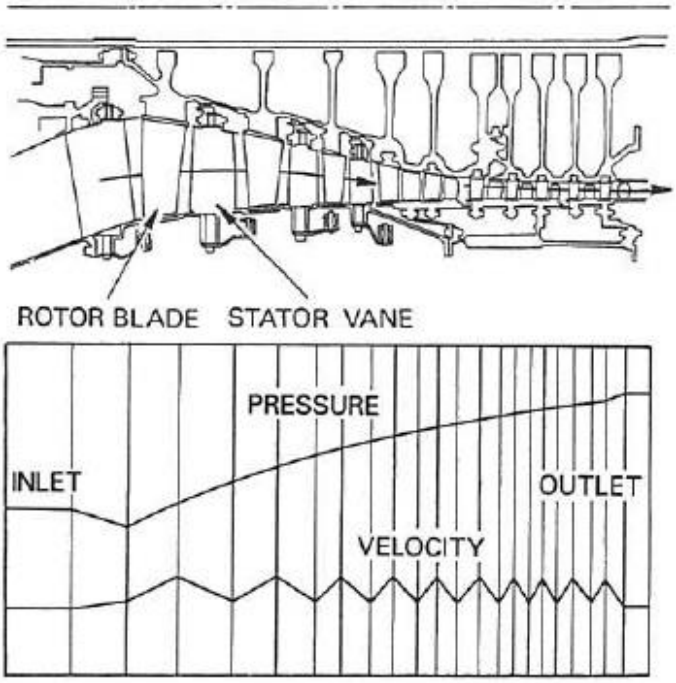

Figure 4 Pressure and velocity profiles through an axial compressor [3]

1.1.3. Combustion

In the combustion chamber, a large amount of liquid fuel is burned. The liquid fuel is supplied through nozzles, whilst the extensive volumes of air are supplied by the compressor and entrained through the air channels. The liquid fuel evaporates and the heat is released in such manner that the hot gas mixture is expanded and accelerated. One of the conditions put upon the jet engine combustion chambers is to achieve a smooth stream of uniformly heated gas on the entrance of the engine turbine. The air from the engine compressor enters the combustion chamber with high velocity. Due to low kerosene burning speed, only a few meters per second, a region characterised with low axial velocity must be created. This is usually achieved by using the air swirler with the main function to curve the air trajectories.

1.1.3.1. Combustion chamber design

Each combustion chamber contains flame tube and air casing used for introducing the cold air. The cold air is used for cooling the flame tube walls and hot gas mixture, as shown in Figure 5.

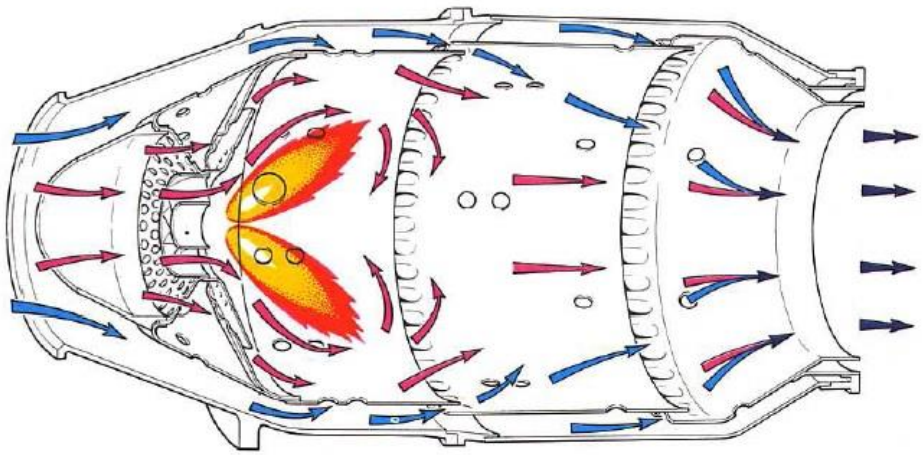

Figure 5 Airflow pattern [3]

In this thesis, three types of combustion chamber are described:

1. Multiple combustion chamber – where several can shaped chambers are disposed around the engine. Each one has an inner flame tube around which air casing is placed, as shown in Figure 6. The main advantage of this design is relatively simple and cheap maintenance.

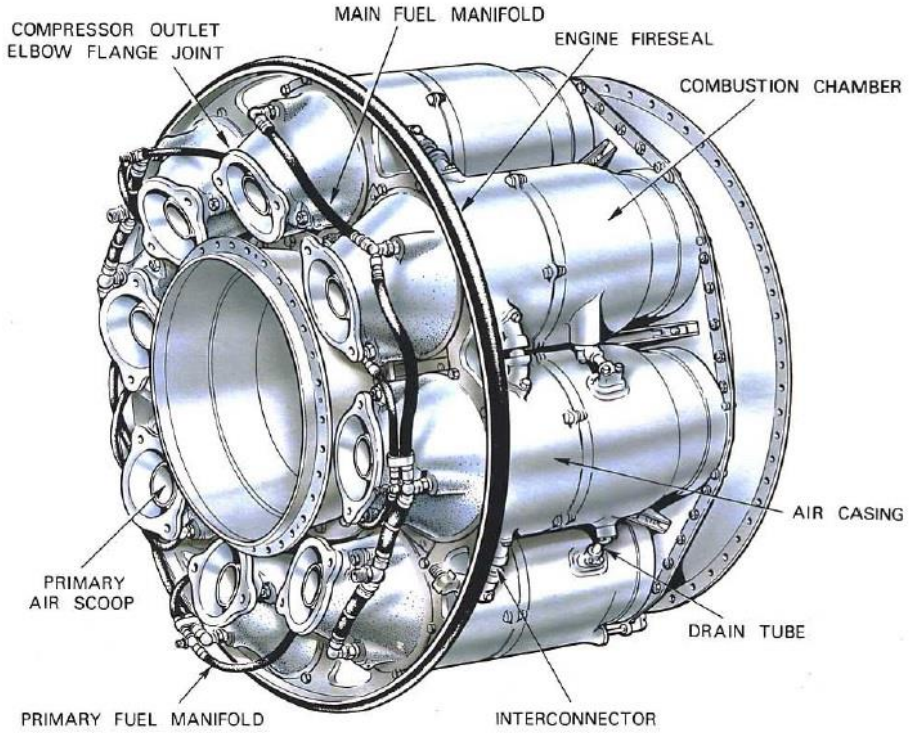

Figure 6 Multiple combustion chamber [3]

2. Tubo-annular combustion chamber – which represent transition design between the multiple and annular types. In such design, a several can shaped chambers are fitted inside a common air casing, as shown in Figure 7. The design combines the ease of maintenance with the compactness of the annular system.

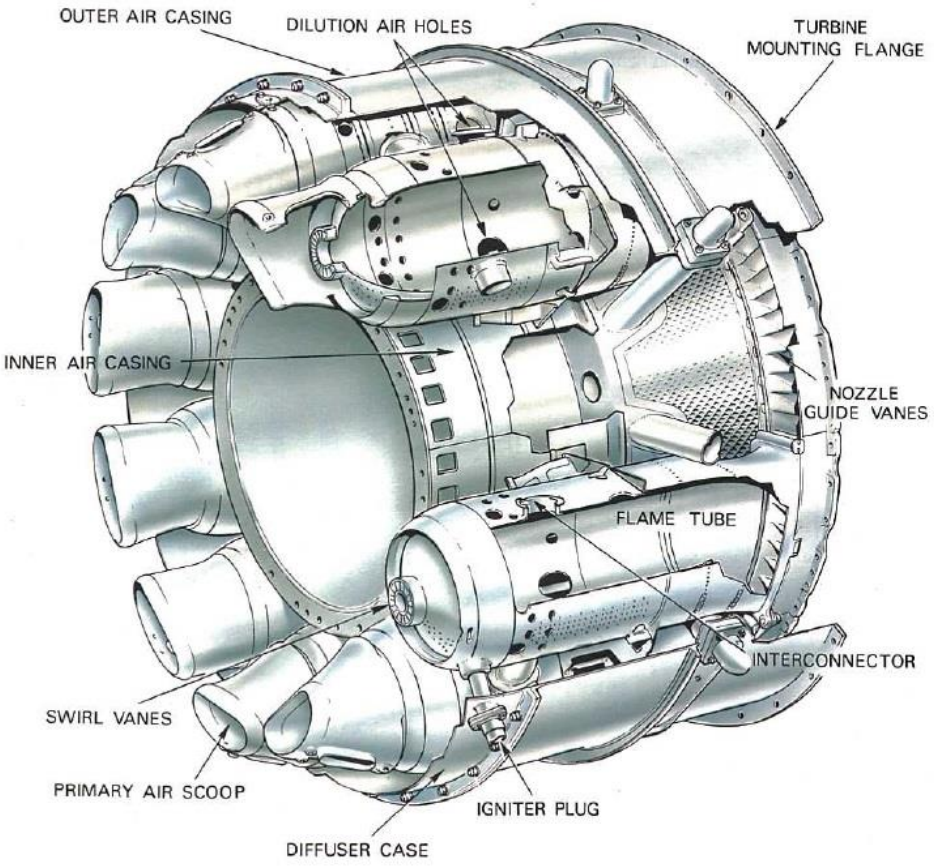

Figure 7 Tubo-annular combustion chamber [3]

3. Annular combustion chamber – which have a single flame tube, completely annular in form as shown in Figure 8. The main advantage of such design is that, for the same power output, the length of the chamber is only 75% of the corresponding tubo-annular combustion chamber. On the other hand, the disadvantage of such combustion chamber is a more complicated and expensive maintenance.

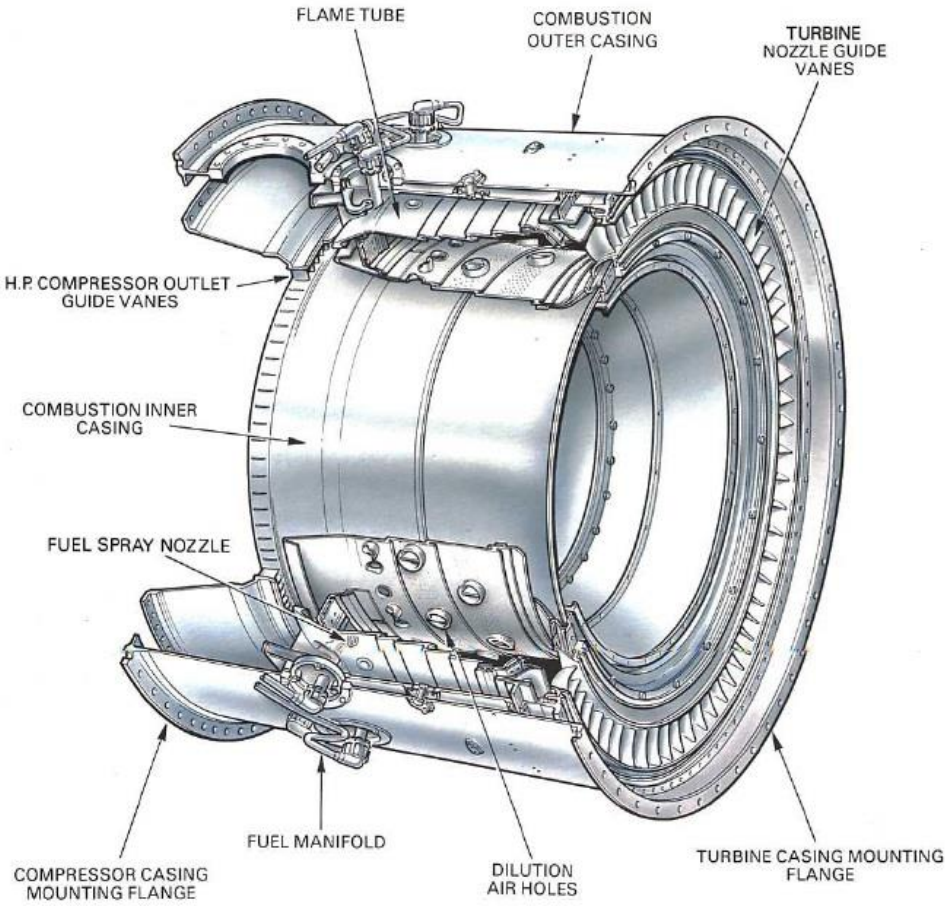

Figure 8 Annular combustion chamber [3]

1.1.3.2. Fuel spray nozzle

The function of fuel spray nozzle is to atomize the liquid fuel which ensures a rapid vaporisation and subsequent fuel burning. The main problem encountered in the observed engineering application is to achieve a proper atomization for a wide range of engine operating points. In this thesis, five different nozzle design are described:

1. The Simplex – first use was on the early jet engine concept. Such nozzle consists of a chamber, which induces a swirled motion into the fuel, and a fixed-area atomizing orifice. This nozzle provides a good atomization at higher fuel pressure, but it has disadvantages at the low pressures, characteristic for low engine speeds and high altitudes.

2. Lubbock – this nozzle design uses a spring-loaded piston to control the area of the inlet to the swirl chamber. At low fuel flows the ports are partly uncovered by the movement

of the piston, and at the high flows they are fully open. By this method, a good atomization is maintained over a wide range of fuel flows. This nozzle isn't widely used today because it was superseded by the Duplex nozzle.

3. Duplex – requires the two fuel manifold, each with an independent orifice. One orifice is much smaller than the other. The smaller orifice handles the lower fuel flows and larger orifice operates at higher fuel flow as the fuel pressure increases.

4. The spill type – similar to the simplex nozzle but designed with a passage extending from the swirl chamber. This passage is used for spilling fuel away at low fuel flows.

5. The airspray nozzle – this nozzle is designed to utilise the high velocity air supplied by the compressor for atomization of the fuel spray. Using the airspray nozzle, the local fuel-rich region are avoided, thus resulting in reduction of carbon formation and exhaust smoke. Another advantage of the airspray nozzle is a lower fuel pressure and a lighter fuel pump.

1.1.4. Exhaust

After the gas mixture is formed in the combustion chamber, it outflows from the engine through the turbine and propelling nozzle. Turbine extracts energy from hot gas mixture required for running the compressor. As the hot gas mixture outflow through the propelling nozzle, it produces thrust.

1.2. Computational fluid dynamics

CFD is widely used for numerical modelling of various reactive processes, for example [4–6]. Using CFD in combination with experimental research has become a standard approach in the development of engineering systems. In aerospace application, CFD tools are used for modelling the turbulence and combustion processes, aero-acoustics, geometry definition, etc. [7]. With the CFD simulation the detailed output data which include temperature fields, evaporated fuel and emission concentrations, spray cloud shape, etc. can be obtained. Such information can be further analysed and implemented on real designs to improve existing combustion chambers. One of a significant factor which influences on the efficiency of combustion process is fuel spray [8][9]. The fuel spray characteristics, such as spray angle,

number of nozzle holes, types of spray nozzle, droplet diameter, etc. determine the efficiency of combustion process [10][11][12]. Therefore, a mathematical model which describe proper chemical and physical behaviour of spray must be used. In this research, the Euler Lagrangian approach was used for spray modelling. The Euler Lagrangian approach treats the gas phase as a continuum, whilst the liquid phase is treated by using the Lagrangian formulation [13]. The combustion process was modelled with the ECFM-3Z model, whilst the spark ignition was modelled with Imposed Stretch Spark Ignition Model (ISSIM) spark ignition model. The ECFM-3Z model is extended coherent flame model that can be used together with the mentioned spark ignition model [14].

2. MATHEMATICAL MODEL

In this section, the used mathematical models are described. Initially, the main transport equations for CFD are presented. Further, the $k-\zeta-f$ turbulence model equations are described. For spray development, the Euler Lagrangian approach was employed, whilst for the combustion process, the advanced ECFM-3Z combustion model was used in combination with the ISSIM ignition model. At the end of this section, the model used for NO_x emission production is shown.

2.1. Conservation law for a control volume

The main assumption of the mathematical models in this thesis is that the gas phase inside the combustion chamber is regarded as continuum, where properties such as density, pressure, velocity, etc. are defined as averages over domain elements, neglecting the behaviour of individual molecules. The fundamental equations that describe the continuum are based on the conservation laws of mass (Equation of Continuity), momentum (Newton's second law) and energy (The first Law of Thermodynamics). They are obtained by using the finite volume approach where the observed domain is divided into a number of control volumes and a mathematical description is developed for the finite control volume.

2.1.1. Mass conservation equation

In a case of single phase fluid flow, the fluid mass in a control volume cannot be created or destroyed. The mass within the control volume will increase if the inflow is higher than the outflow, and in the opposite case, it will decrease. If there are no volume or surface sources, the integral form of mass conservation for the control volume can be written as:

$$\int_S \rho\, u_i\, n_i\, dS = -\frac{\partial}{\partial t}\int_V \rho\, dV. \tag{2.1}$$

The mass flux through element boundary surface S is represented on the left-hand side of equation (2.1), whilst the term on the right-hand side denotes the rate of change of total mass in the control volume V.

2.1.2. Momentum conservation equation

According to Newton's second law, the conservation of momentum is derived. The rate of momentum change of a fluid particle is equal to the sum of the volume and surface forces acting on the particle. The integral form of momentum conservation for a fixed spatial control volume V can be written as:

$$\int_V \frac{\partial}{\partial t}(\rho\, u_j)\, dV + \int_S (\rho\, u_j)\, u_i\, n_i\, dS = \int_V \rho\, f_j\, dV + \int_S \sigma_{ij}\, n_i\, dS. \tag{2.2}$$

The conservation of momentum represents a vector equation that comprises three momentum equations ($j = 1, 2, 3$). Each equation describes the values of momentum change in Cartesian coordinate system. The first term on the left-hand side of equation (2.2) represents the rate of momentum change in the control volume *V*. The second term on the left-hand side represents the net momentum flux across the control volume boundaries *S*. The right-hand side of equation (2.2) is the sum of volume and surface forces acting on fluid within the control volume. The first term denotes the volume forces such as gravitational, centrifugal forces, etc. The second term denotes the surface forces which can be decomposed in two components, pressure forces and viscous stress forces, defined as:

$$\sigma_{ij} = -p\, \delta_{ij} + \tau_{ij}. \tag{2.3}$$

In equation (2.3) the term p is absolute pressure, δ_{ij} is the Kronecker delta which is equal to 1 if $i = j$ and 0 if $i \neq j$, and τ_{ij} is viscous stress. In a Newtonian fluid the viscous stress tensor τ_{ij} is linearly proportional to the rate of deformation:

$$\tau_{ij} = \mu \left(\frac{\partial u_i}{\partial x_j} + \frac{\partial u_j}{\partial x_i}\right) - \frac{2}{3}\, \mu\, \frac{\partial u_k}{\partial x_k}\, \delta_{ij}, \tag{2.4}$$

where μ is homogeneous fluid viscosity. Taking into account the equations (2.3) and (2.4) the momentum conservation equation can be written as:

$$\int_V \frac{\partial}{\partial t}(\rho\, u_j)dV + \int_S (\rho\, u_j)\, u_i\, n_i\, dS = \int_V \rho\, f_j\, dV - \int_S p\, n_i\, dS + \int_V \mu\, \frac{\partial^2 u_i}{\partial x_i \partial x_i}\, dV. \quad (2.5)$$

Equations (2.1) and (2.5) are known as the Navier-Stokes equations.

2.1.3. Energy conservation equation

The energy equation is derived by following the physical principle that the amount of energy cannot be created or destroyed, it can only be converted from one form to another and the total energy within the domain remains constant. The conservation of energy is derived from the First law of thermodynamics. The change in rate of energy equals to the sum of the rate of heat addition and the rate of work done on the fluid particle. The integral form of energy conservation equation can be written as:

$$\int_V \frac{\partial}{\partial t}(\rho e)\, dV + \int_S (\rho e) u_i\, n_i dS = \int_V \rho\, f_i\, u_i\, dV + \int_V S_e dV + \int_S \sigma_{ij}\, u_i\, n_j\, dS - \int_S q_i\, n_i\, dS. \quad (2.6)$$

The first term on the left-hand side of equation (2.6) represents the rate of total energy increase, while the second term represents the total energy exchanged across the control volume boundaries. The first term on the right-hand side is the specific power generated by the volume forces f_i, in the second term S_e denotes the distributed internal heat source/sink due to radiation, chemical reactions or any other volumetric heat source. The third term on right-hand side of equation (2.6) denotes the surface sources, which are consisting of work done by the pressure and viscous stresses acting on the fluid element. The last term denotes the heat flux vector, which can be written in the form of Fourier's law of heat conduction:

$$q_i = -\lambda\, \frac{\partial T}{\partial x_i}. \quad (2.7)$$

Equation (2.7) shows that the heat flux vector is linearly related to the temperature gradient where the term λ is the thermal conductivity coefficient.

2.1.4. Species mass conservation equation

In a case of combustion process, the conservation equation for each of the chemical species of interest is required. The integral form of species mass conservation can be written as:

$$\int_V \frac{\partial}{\partial t}(\rho Y_k)\, dV + \int_S (\rho Y_k)\, u_i\, n_i\, dS = \int_S (\rho\, \Gamma_k\, \frac{\partial Y_k}{\partial x_i})\, n_i\, dS + \int_V S_k\, dV, \tag{2.8}$$

where Y_k is the mass fraction of the *k*-th chemical species defined as:

$$Y_k = \frac{m_k}{m}. \tag{2.9}$$

In equation (2.9) term m_k is the mass of species k, and m is the total mass. The first term on the right-hand side of equation (2.8) is the diffusion term which is modelled by Fick's law of diffusion that is an analogue to Fourier's law in equation (2.7). The diffusion term Γ_k is called the diffusion coefficient. The last term on the right-hand side is the source/sink term due to chemical reactions.

2.1.5. General transport equation

Fundamental physical conservation laws which are described above in their original forms are defined as an equilibrium for a control volume. General transport equation of some extensive property can be written as:

$$\underbrace{\int_V \frac{\partial}{\partial t}(\rho\varphi)dV}_{Unsteady\ term} + \underbrace{\int_S (\rho\varphi)\, u_i\, n_i\, dS}_{Convection} = \underbrace{\int_S \left(\Gamma_\varphi \frac{\partial \varphi}{\partial x_i}\right) n_i\, dS}_{Diffusion} + \underbrace{\int_V S_\varphi\, dV}_{Source/Sink}. \tag{2.10}$$

The first term on the left-hand side represents the rate of change of the scalar properties φ in the control volume, and the second term is the net convective flux of this property across the control volume boundaries. The first term on the right-hand side is the net diffusive flux across the control volume boundaries, and the second term is the source or sink of the property φ.

It is necessary to emphasize that equation (2.10) is very important and it is used as a base and starting point for computational procedures in the finite volume CFD approach.

2.2. Turbulence model

Turbulent flow is represented in almost all engineering applications, and it is characterised by a broad range of temporal and spatial scale. Therefore, direct solving of turbulent flow is theoretically possible, but it requires a fine mesh with a high number of computational cells and small time steps. This approach is currently too expensive for calculating spray and combustion processes in a real engineering applications [8]. For this reasons, in this research, Reynolds Averaged Navier Stokes (RANS) equation approach was used where all turbulent eddies are being modelled by means of the turbulence models. In such approach, the instantaneous variables of turbulent flow quantities are replaced with the time averaged value and its fluctuating part. Additionally, two terms are introduced into the conservation equations: the Reynolds stress tensor and the turbulent heat flux which results from the averaging processes. In order to solve a turbulent flow, those terms have to be modelled which is done by means of turbulence models. In this research, the $k-\zeta-f$ model was used because of its advantage in robustness for modelling strong swirling flows that are characteristic for the observed application.

2.2.1. $k-\zeta-f$ turbulence model

The used turbulence model was developed by Hanjalić, Pupovac and Hadžiabdić [15]. The turbulence model is based on Durbin's elliptic relaxation concept [16]. The aim of the authors was to improve the numerical stability of the original $\overline{v^2}-f$ model by solving a transport equation for the velocity scale ratio $\zeta = {\overline{v^2}}/{k}$ instead of velocity scale $\overline{v^2}$. The eddy-viscosity term is calculated with equation:

$$v_t = C_\mu \, \zeta \, \frac{k^2}{\varepsilon}, \tag{2.11}$$

where C_μ is the turbulent model constant, k is turbulent kinetic energy and ε is the rate of turbulent energy dissipation. The rest of variables can be obtained with following set of equation [17]:

$$\rho \frac{Dk}{Dt} = \rho \left(P_k - \varepsilon\right) + \frac{\partial}{\partial x_j}\left[\left(\mu + \frac{\mu_t}{\sigma_k}\right)\frac{\partial k}{\partial x_j}\right], \tag{2.12}$$

$$\rho \frac{D\varepsilon}{Dt} = \rho \frac{C_{\varepsilon 1}^{*} P_K - C_{\varepsilon 2}\varepsilon}{T} + \frac{\partial}{\partial x_j}\left[\left(\mu + \frac{\mu_t}{\sigma_\varepsilon}\right)\frac{\partial \varepsilon}{\partial x_j}\right], \tag{2.13}$$

$$\rho \frac{D\zeta}{Dt} = \rho f - \rho \frac{\zeta}{k} P_k + \frac{\partial}{\partial x_j}\left[\left(\mu + \frac{\mu_t}{\sigma_\zeta}\right)\frac{\partial \zeta}{\partial x_j}\right]. \tag{2.14}$$

In equations above f can be calculated:

$$f - L^2 \frac{\partial^2 f}{\partial x_i \partial x_j} = \left(C_1 + C_2 \frac{P_k}{\zeta}\right)\frac{\left(\frac{2}{3} - \zeta\right)}{T}, \tag{2.15}$$

and turbulent time scale T and length scale L are given by:

$$T = \max\left(min\left(\frac{k}{\varepsilon}, \frac{a}{\sqrt{6}C_\mu |S|\zeta}\right), C_T\left(\frac{\nu}{\varepsilon}\right)^{1/2}\right), \tag{2.16}$$

$$L = C_L \max\left(min\left(\frac{k^{3/2}}{\varepsilon}, \frac{k^{1/2}}{\sqrt{6}C_\mu |S|\zeta}\right), C_\eta \frac{\nu^{3/4}}{\varepsilon^{1/4}}\right). \tag{2.17}$$

Additional modification to the equation is that the constant $C_{\varepsilon 1}$ close to the wall can be calculated as:

$$C_{\varepsilon 1}^{*} = C_{\varepsilon 1}\left(1 + 0.045\sqrt{\frac{1}{\zeta}}\right). \tag{2.18}$$

The empirical constant in this model are not universal and must be adjusted for a particular problem. In this research, set of default values in CFD solver AVL FIRE™ was used, and it is given in Table 1:

Table 1 The default values of the $k-\zeta-f$ turbulence model in AVL FIRE™

C_μ	$C_{\varepsilon 1}$	$C_{\varepsilon 2}$	C_1	C_2	σ_k	σ_ε	σ_ζ	C_T	C_L	C_η
0.22	1.4(1+0.012/ζ)	1.9	0.4	0.65	1	1.3	1.2	6	0.36	85

2.3. Spray modelling

Spray simulation involves a multi-phase flow phenomena and as such require numerical solution of conservation equations for the gas and the liquid phase simultaneously. With respect to the liquid phase, most spray calculations in the engineering environment today are based on a statistical method referred as Discrete Droplet Method (DDM). DDM operates by solving ordinary differential equations for the trajectory, momentum, heat and mass transfer of single droplet, each being a member of a group of identical non-interacting droplets termed a *'parcel'.* Thus one member of the group represents the behaviour of the complete parcel.

During the fuel injection through a small diameter nozzle into the combustion chamber, fuel is exposed to aerodynamic and turbulent forces. This leads to fuel disintegration into smaller droplets of different shapes and sizes, and into unstable ligaments. This disintegration process is called the spray process. It is a common knowledge that characteristic of spray influences on fuel/air mixing, evaporation and combustion process and thus, the overall combustion chamber efficiency [8].

The spray momentum equation describes that the change in droplet momentum is equal to the drag force which acts on the droplet:

$$m_p \frac{du_{ip}}{dt} = F_{idr}. \tag{2.19}$$

In equation (2.19) the term m_p stands for the mass of a parcel, whilst the F_{idr} is the drag force.

In this thesis, two sub-models were used for spray modelling. The first model is WAVE break-up model which describe the disintegration model of spray droplets, whilst for the evaporation of the liquid droplets, the Abramzon-Sirignano evaporation model was utilised.

2.3.1. WAVE break-up model

In this research, the WAVE model was used to model the disintegration process. There are two type of break-up regimes, Kevin-Helmholtz (KH) regime which is specified for high velocity, and Rayleigh-Taylor (RT) regime which is specified for low velocities. The high relative velocity between liquid droplets and the surrounding gas results in the occurrence of unstable surface waves. The growth of such waves on the parent droplets results in mass detachment and in the creation of new, smaller diameter droplets. In Equation (2.20) the correlation between radius of created droplet r_{stable} and the wavelength Λ of the fastest growing surface wave is shown. In this thesis, the model constant C_1 was set to recommended value of 0.61 [18].

$$r_{stable} = C_1 \Lambda. \tag{2.20}$$

The time, τ_a, necessary for disintegration process is given in Equation (2.21):

$$\tau_a = \frac{3.726 C_2 r_k}{\Lambda_k \Omega_k}. \tag{2.21}$$

The second model constant C_2 corrects the characteristic break-up time and varies from one injector to another. The recommended values can vary from 1.73 to 160 [19] where higher values of C_2 slows down the disintegration process. The term r_k in Equation (2.21) is the radius of the parent droplet, whilst Ω_k is the wave growth rate, and the Λ_k is the wave length. Experimental research has been used to derive empirical equations for Ω_k and Λ_k as function of the local flow properties that are based specifically on the Reynolds (*Re*) and the Ohnesorge numbers (*Oh*), which are given in equations (2.22) and (2.23):

$$\Lambda_k = 9.02 r_k \frac{(1 + 0.45\, Oh^{0.5})(1 + 0.4\, T^{0.7})}{(1 + 0.87\, We_1^{1.67})^{0.6}}, \tag{2.22}$$

$$\Omega_k = \left(\frac{\rho_k r_k^3}{\sigma}\right)^{-0.5} \frac{0.34 + 0.38\, We_1^{1.5}}{(1+Oh)(1+1.4\,T^{0.6})}. \tag{2.23}$$

In equations (2.22) and (2.23) the term We_1 is the droplet Weber number, T is the combination of the Ohnesorge and the Weber number equal to $OhWe^{0.5}$, σ is the fuel surface tension and ρ_k is the fuel density.

2.3.2. Abramzon and Sirignano evaporation model

The disintegrated droplets evaporate due to high temperature conditions inside the combustion chamber. The evaporation of fuel was modelled by using the Abramzon evaporation model which assumes uniform droplet temperature distribution and spherical droplet geometry [20]. Abramzon and Sirigano evaporation model relies on the classic film theory where the resistance to the heat and mass transfer are modelled by fictional gas films of constant thickness δ_t and δ_m. In the case of an evaporating droplet, these film thickness values have to be corrected by the factors F_T and F_M [21]. The rate of change of mass can then be described by the Sherwood and by the Nusselt number:

$$\dot{m} = \pi\, \overline{\rho_g}\, \overline{\beta_g}\, D_d\, Sh^*\, ln(1+B_M), \tag{2.24}$$

$$\dot{m} = \pi\, \frac{\overline{k_g}}{\overline{C_{pF}}} D_d Nu^* ln(1+B_T). \tag{2.25}$$

In equations (2.24) and (2.25) the terms $\overline{\rho_g}$, $\overline{\beta_g}$ and $\overline{k_g}$ are the average density, binary diffusion coefficient and thermal conductivity of the gas mixture in the film, and $\overline{C_{pF}}$ is the average vapor specific heat in the film. The Nusselt and Sherwood numbers are the non-dimensional parameters which are expressed as:

$$Sh^* = 2 + \frac{Sh_0 - 2}{F_M}, \tag{2.26}$$

$$Nu^* = 2 + \frac{Nu_0 - 2}{F_T}. \tag{2.27}$$

The values B_M and B_T are called the Spalding mass and heat transfer numbers and they are calculated as:

$$B_M = \frac{Y_{Fs} - Y_{F\infty}}{1 - Y_{Fs}}, \tag{2.28}$$

$$B_T = \frac{\overline{C_{pF}}(T_\infty - T_s)}{L(T_s) + \frac{Q_L}{\dot{m}}}. \tag{2.29}$$

In equations above, Y_F is the fuel mass fraction, and $L(T_s)$ is the latent heat of vaporisation at temperature T_s. In equations (2.28) and (2.29) subscripts s and ∞ refer to the conditions at the droplet surface and external gas flow.

2.4. Combustion modelling

Combustion can be defined as chemical reactions between the fuel and the oxidizer followed with a significant heat release. In this research, ECFM-3Z model was used for combustion modelling. In this combustion model the transport equations are solved for the averaged quantities of chemical species such as: fuel species, O_2, N_2, NO, CO_2, CO, H_2, H_2O, O, H, N, OH inside each computational cell containing three mixing zones, as shown in Figure 9 [22]. Equations are classically modelled as:

$$\frac{\partial \bar{\rho}\widetilde{Y_k}}{\partial t} + \frac{\partial \bar{\rho}\,\widetilde{u_i}\,\widetilde{Y_k}}{\partial t} - \frac{\partial}{\partial x_i}\left(\left(\frac{\mu}{Sc} + \frac{\mu_t}{Sc_t}\right)\frac{\partial \widetilde{Y_k}}{\partial x_i}\right) = \bar{\dot{\omega}}_x, \tag{2.30}$$

where $\overline{\dot{\omega}_x}$ is the combustion source term and $\widetilde{Y_k}$ is the averaged mass fraction of species *k*.

The fuel is divided into two parts: the fuel present in the fresh gases, $\tilde{Y}_{Fu}^u$ and the fuel present in the burnt gases, $\tilde{Y}_{Fu}^b$. An additional transport equation is used to compute $\tilde{Y}_{Fu}^u$:

$$\frac{\partial \bar{\rho}\tilde{Y}_{Fu}^{u}}{\partial t}+\frac{\partial \bar{\rho}\,\widetilde{u_i}\,\tilde{Y}_{Fu}^{u}}{\partial t}-\frac{\partial}{\partial x_i}\left(\left(\frac{\mu}{Sc}+\frac{\mu_t}{Sc_t}\right)\frac{\partial \tilde{Y}_{Fu}^{u}}{\partial x_i}\right)=\bar{\rho}\,\tilde{\dot{S}}_{Fu}^{u}+\bar{\dot{\omega}}_{Fu}^{u}, \tag{2.31}$$

where $\tilde{\dot{S}}_{Fu}^{u}$ is the source term quantifying the fuel evaporation in fresh gases and $\bar{\dot{\omega}}_{Fu}^{u}$ is a source term taking ignition and mixing between mixed unburned and mixed burnt areas into account.

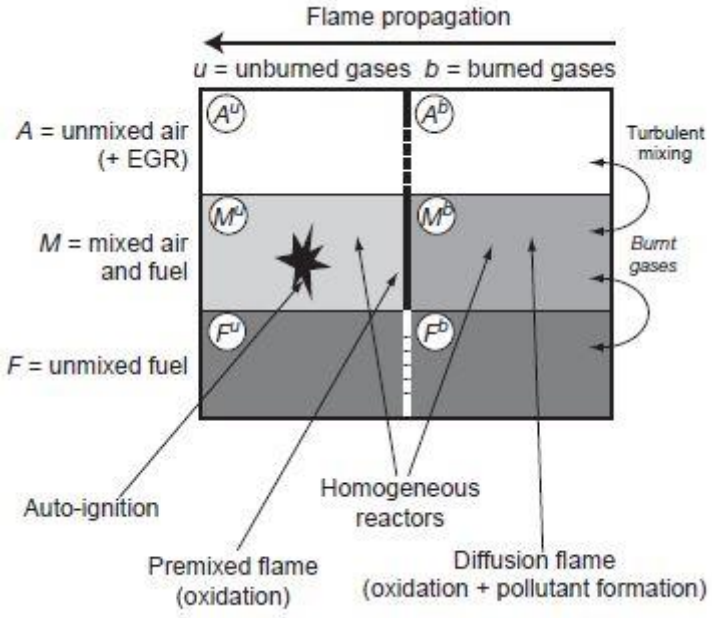

Figure 9 Schematic of the ECFM-3Z model computational cell [22]

For modelling ignition, the ISSIM model was used in this research. At ignition timing, an initially burned gas profile is created. Then, the rate of reaction is directly controlled by the Flame Surface Density (FSD) equation [14] for which the source term are modified to correctly represent flame surface growth during the ignition.

2.5. Emission modelling

This chapter describes the mathematical model for simulation of nitric oxide (NO) formation. In thesis, NO formation from two principle sources are taken into account:

- Thermal NO which is formed due to dissociation of the molecular air-nitrogen**;**
- Prompt NO formed by "attack" of hydrocarbon fragments on the air-nitrogen;

2.5.1. Thermal NO mechanism

The thermal NO mechanism involves a reaction between atmospheric nitrogen and the atomic oxygen produced in the high temperature regions of the flame. The major factors that influence thermal NO formation are temperature, atomic oxygen, concentrations of nitrogen, and residence time. Of these four factors, the temperature is the most important because atmospheric nitrogen has a strong triple bond and is extremely stable. Thus, it can be only decomposed at the very high temperature within the flame. The production of NO is significant at temperatures exceeding approximately $1550\ °C$ due to the high activation energy. At the temperatures lower than $1000\ °C$, the amount of thermal NO is reduced, while at temperatures below $760\ °C$ NO is generated in much lower concentrations or not at all [23].

The process of NO formation be determined by a set of chemical reactions, which was firstly described by Zeldovich (1946) as a two-step mechanism and later extend with additional elementary reactions:

$$N_2 + O \overset{k_1}{\leftrightarrow} NO + N, \tag{2.32}$$

$$N + O_2 \overset{k_2}{\leftrightarrow} NO + O, \tag{2.33}$$

$$N_2 + OH \overset{k_3}{\leftrightarrow} NO + H. \tag{2.34}$$

The first two reactions (2.32) and (2.33) were originally proposed by Zeldovich and extended later by including the third reaction (2.34). It was observed that the nitrogen atoms released at reactions (2.34) are oxidized to nitric oxide mainly by hydrogen radicals at near-stoichiometric conditions and in fuel-rich mixtures.

The temporal change and of NO concentrations is given by:

$$\frac{dc_{NO}}{dt} = k_{1f}c_O c_{N_2} + k_{2f}c_N c_{O_2} + k_{3f}c_N c_{OH} - k_{1b}c_{NO}c_N - k_{2b}c_{NO}c_O - k_{3b}c_{NO}c_H, \tag{2.35}$$

considering forward and backward directions where the concentrations c are given in mol/cm^3, and reaction rate coefficients $k_{1f}, k_{2f}, k_{3f}, k_{1b}, k_{2b}$, and k_{3b} for the forward and corresponding backward reactions can be expressed according to Arrhenius law [24]:

$$k = AT^{\beta} \exp\left(-\frac{E}{RT}\right). \tag{2.36}$$

The coefficient A, β and E are determined from experimental data, and E is activation energy. First expression, AT^{β} is coefficient of reaction speed, and represents frequency of molecular collision. Second expression $\exp\left(-\frac{E}{RT}\right)$ is Boltzmann's factor and represents which molecules have achieved required energy for reaction.

The overall NO formation rate for these three reactions can be expressed as:

$$\frac{dc_{NO}}{dt} = 2\, k_{1f}\, c_O\, c_{N_2} \frac{\left(1 - \frac{k_{1b}\, k_{2b}\, c_{NO}^2}{k_{1f}\, c_{N_2}\, k_{2f}\, c_{O_2}}\right)}{1 + \frac{k_{1b}\, c_{NO}}{k_{2f}\, c_{O_2}}}. \tag{2.37}$$

2.5.2. Prompt NO mechanism

Fenimore was the first who identified this NO formation mechanism [25]. Prompt NO becomes important at low temperatures (below $800\ °C$), fuel-rich mixtures, and short residence time. Prompt NO is formed by the reactions of atmospheric nitrogen with hydrocarbon fragments, which is subsequently oxidised to form NO. Initiating steps for prompt NO, from fuel CH, are reactions shown in a set of equations (2.38), whilst for fuel CH_2, reaction is shown in equation (2.39):

$$\begin{gathered} CH + N_2 \leftrightarrow HCN + N \\ N + O_2 \leftrightarrow NO + O \\ HCN + OH \leftrightarrow CN + H_2O \\ CN + O_2 \leftrightarrow NO + CO, \end{gathered} \tag{2.38}$$

$$CH_2 + N_2 \leftrightarrow HCN + NH. \tag{2.39}$$

In the early stage of the flame development, where Prompt NO is formed under fuel-rich conditions, the O concentration is high and N radicals almost exclusively forms NO rather than nitrogen. Therefore, the prompt NO formation rate will be approximately equal to the overall prompt NO formation rate:

$$\frac{dc_{NO}}{dt} = A\, f\, c_{O_2}^{b}\, c_{N_2}\, c_{fuel} \exp\left(-\frac{E}{RT}\right), \tag{2.40}$$

where *c* denotes the concentrations, *k* is the pre-exponential factor, *f* is the correction factor, *b* is the order of reaction for molecular oxygen and *E* is the activation energy.

2.5.3. Chemistry-Turbulence interaction

Combustion processes typically occur in a turbulent environment, which requires special consideration when predicting NO concentrations. There is a difference between the NO profiles predicted using the mean temperature and densities, and profiles predicted by the temperature and density fluctuations caused by turbulence [23]. Therefore, it is important to incorporate the effects of the turbulent fluctuations on the presented NO pollutant reaction process. Time-mean reaction rates of NO cannot be calculated from the time-mean value of temperature because the relationship among NO kinetic rates and temperatures are highly nonlinear. The presumed probability density function (PDF) approach is used in order to take into account the effects of turbulent fluctuations on the NO kinetic rates. These rates are integrated with respect to the fluctuation temperature like:

$$\overline{S_{NO}} = \int_0^1 P(T)\, S_{NO}(T)\, dT, \tag{2.41}$$

where $P(T)$ is the probability density function of the normalised temperature T, and S_{NO} is the instantaneous NO source. The PDF is assumed to be a two-moment beta function, which is suitable for the combustion calculations. The beta probability density function for a given value T, and a given pair of values α and β is:

$$P(T) = \frac{1}{B(\alpha,\beta)} T^{\alpha-1}(1-T)^{\beta-1}, \tag{2.42}$$

where $B(\alpha,\beta)$ is beta function. Equation (2.42) computes the probability density $P(T)$ at T for a beta distribution with parameters α and β which must be positive, and the value T must lie on the interval [0, 1]. Thus, this variable T must be normalised. The beta function is defined as:

$$B(\alpha,\beta) = \int_0^1 T^{\alpha-1}\,(1-T)^{\beta-1}\,dT, \tag{2.43}$$

where the beta function can be also defined as:

$$B(\alpha,\beta) = \frac{\Gamma(\alpha)\Gamma(\beta)}{\Gamma(\alpha+\beta)}. \tag{2.44}$$

The gamma function of some variable z is defined the integral:

$$\Gamma(\mathrm{z}) = \int_0^\infty e^{-t}\,t^{z-1}\,dT. \tag{2.45}$$

Parameters α and β depend on the mean value of the temperature from the main combustion calculation and its variance $\widetilde{T''^2}$:

$$\alpha = \tilde{T}\left[\frac{\tilde{T}(1-\tilde{T})}{\widetilde{T''^2}} - 1\right], \tag{2.46}$$

$$\beta = (1-\tilde{T})\left[\frac{\tilde{T}(1-\tilde{T})}{\widetilde{T''^2}} - 1\right]. \tag{2.47}$$

Since the parameters α and β must always be positive, $\tilde{T}$ is also positive. The requirement that $\alpha > 0$ shows that $\widetilde{T''^2} < \tilde{T}(1-\tilde{T})$. This requirement is the upper limit of the temperature variance $\widetilde{T''^2}$. The lower limit of the temperature variance must be that $\widetilde{T''^2} > 0.002$, enabling calculation of gamma function. The temperature variance $\widetilde{T''^2}$ can be calculated by solving the transport equation during the combustion calculation stage, or after the main combustion calculation has been completed.

$$\frac{\partial}{\partial t}\left(\bar{\rho}\,\widetilde{T''^2}\right) + \frac{\partial}{\partial x_i}\left(\bar{\rho}\tilde{u}_i\,\widetilde{T''^2}\right) = \frac{\partial}{\partial x_i}\left(\bar{\rho}\frac{\nu_t}{\sigma_t}\frac{\partial \widetilde{T''^2}}{\partial x_i}\right) + 2\bar{\rho}\frac{\nu_t}{\sigma_t}\left(\frac{\partial \tilde{T}}{\partial x_i}\right)^2 - 2\bar{\rho}\frac{\tilde{\varepsilon}}{\tilde{k}}\widetilde{T''^2}, \qquad (2.48)$$

where the constant $\sigma_t = 0.85$ [23]. Equation (2.41) must be integrated at every node and at every iteration. The number of points of the beta function integral is specified by user. A larger number of points yields a more accurate calculation of PDF function, but takes longer to compute.

2.6. Standard species transport model

Species transport can be calculated with two approaches:

- General Species Transport Model;
- Standard Species Transport Model.

In General Species Transport Model, for each chemical species k, transport equation must be calculated. This approach are much time consuming, so in order to reduce the number of equations to be solved, standard species transport is utilised which use dimensionless quantities for describing chemical reactions.

Standard Species Transport Model solves three transport equation [17] for:

- Fuel mass fraction, y_{fu};
- Fuel mixture fraction, f;
- Residual gas mass fraction, g;

Fuel mass fraction is defined as the fraction of the unburned fuel mass, $m_{fu,u}$ and the total mixture mass, m_{total}:

$$y_{fu} = \frac{m_{fu,u}}{m_{total}}. \tag{2.49}$$

Fuel mixture fraction, f is defined as the sum of unburned fuel mass, $m_{fu,u}$ and the mass of the fuel in burnt phase, $m_{fu,b}$, divided by the total mixture mass, m_{total}:

$$f = \frac{m_{fu,u} + m_{fu,b}}{m_{total}}. \tag{2.50}$$

The last term residual gas mass fraction, g is given by:

$$g = \frac{m_{rg}}{m_{rg} + m_{air}}, \tag{2.51}$$

where m_{rg} is mass of residual gas. The three mentioned transport equation can be expressed as:

$$\frac{\partial}{\partial t}(\rho y_{fu}) + \frac{\partial}{\partial x_i}(\rho y_{fu} u_i) = \frac{\partial}{\partial x_i}\left(\Gamma_{fu} \frac{\partial y_{fu}}{\partial x_i}\right) + S_{fu}, \tag{2.52}$$

$$\frac{\partial}{\partial t}(\rho f) + \frac{\partial}{\partial x_i}(\rho u_i f) = \frac{\partial}{\partial x_i}\left(\Gamma_f \frac{\partial f}{\partial x_i}\right), \tag{2.53}$$

$$\frac{\partial}{\partial t}(\rho g) + \frac{\partial}{\partial x_i}(\rho u_i g) = \frac{\partial}{\partial x_i}\left(\Gamma_g \frac{\partial g}{\partial x_i}\right). \tag{2.54}$$

The source term in Equation (2.52) is reaction rate determined in combustion model. The system contains five chemical species: fuel species, O_2, N_2, CO_2 and H_2O, but only for fuel species transport equation is solved. The mass fractions of other chemical species are calculated from stoichiometric equations for complete combustion.

3. SETUP

The numerical simulations were performed with the commercial 3D CFD software AVL FIRE™. In this section, the geometry of combustion chamber is shown. Afterwards, setup for mesh dependency test and boundary conditions for all simulations are described. At the end of the section, spray and general numerical setup are described.

3.1. Combustion chamber geometry

In this thesis, the geometry used for generating computational meshes is an artificial can type combustion chamber which consists: double stage radial swirler with single fuel nozzle and liner without dilution holes. CAD model of geometry was made in software Solidworks [26] and it is shown in Figure 10 together with selections which are later used for boundary conditions in the computer simulations. The CAD model was imported into the CFD tool AVL FIRE™ and computational meshes were generated by using the AVL automatic mesher. Characteristic dimensions of the combustion chamber are shown in Figure 11.

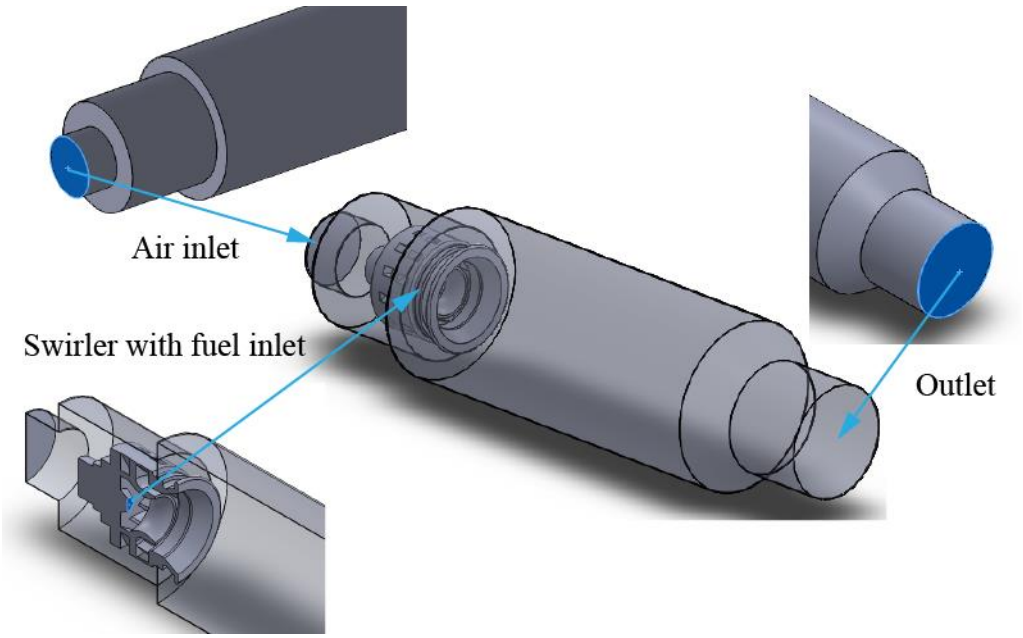

Figure 10 Combustion chamber CAD model

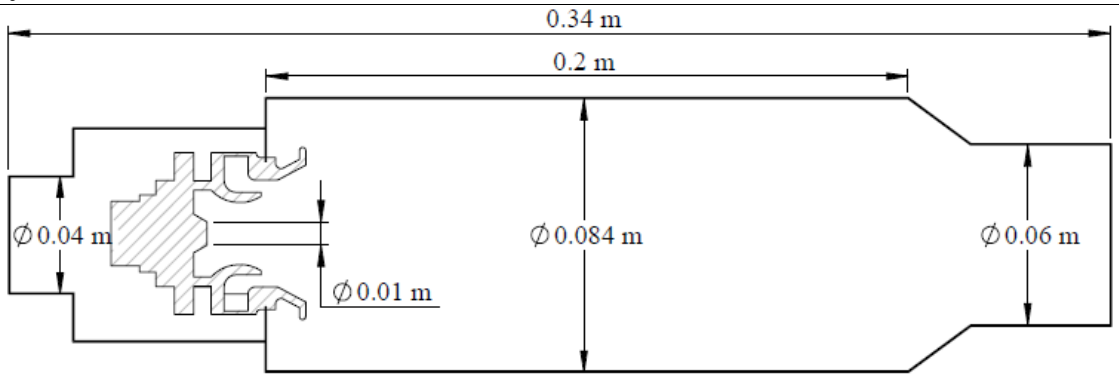

Figure 11 Combustion chamber dimensions

3.2. Mesh dependency setup

In every CFD research mesh dependency test is performed to choose the discretisation level which provides the optimal choice between solution accuracy and computational time. The computational mesh should have minimal number of cells which retains satisfying results. In this research, three different meshes were observed. In Table 2 the specifications for observed computational meshes are listed, where minimal cell size, maximal cell size, and total number of control volumes are shown.

Table 2 Mesh characteristic

Mesh	Minimal cell size [m]	Maximal cell size [m]	Total number of cells
Rough	0.0008025	0.00321	336042
Medium	0.0006581	0.00263	460415
Fine	0.0005062	0.002025	701823

Section of the computational domain around the swirler, for all three meshes is shown in Figure 12. It is visible that the finer mesh has more control volume placed in vicinity of the swirler.

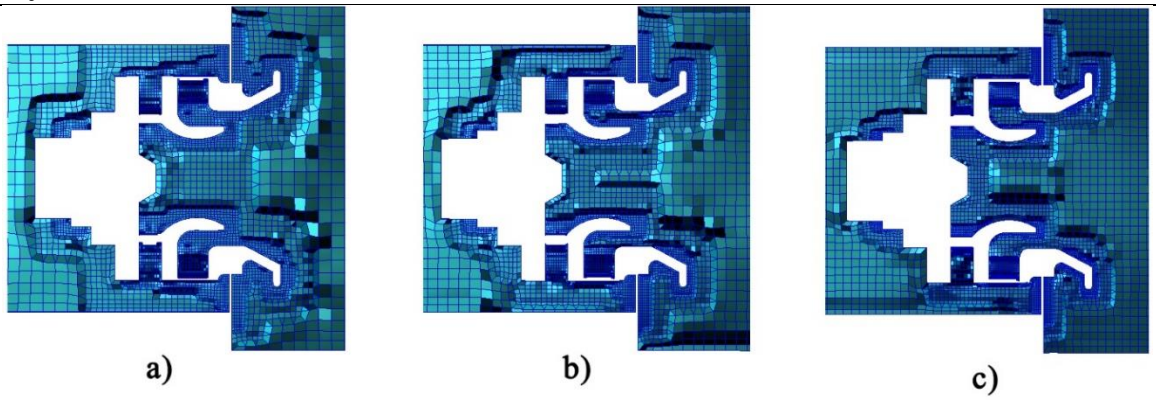

Figure 12 Control volume distribution around swirler a) rough, b) medium, c) fine

3.3. Boundary and initial conditions

To start the computational simulation, boundary and initial conditions have to be defined. In Figure 13 rough mesh with selections defined for boundary conditions is shown, and the same configuration was used for other observed computational meshes. The air flow through the air inlet selection passes through the swirler region and enters the burning area. The fuel is injected through fuel inlet and it is mixed with swirled air found in the burning area. The fuel/air mixture combusts and exhaust gasses outflow through the combustion chambers outlet selection.

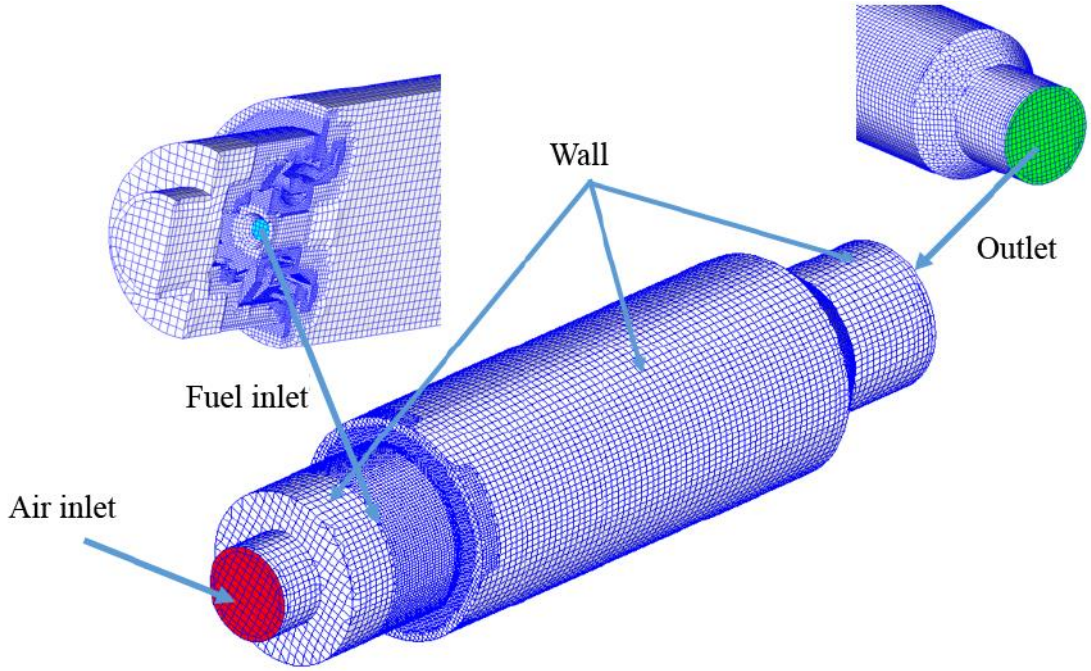

Figure 13 Rough mesh with selections for boundary conditions

The boundary conditions are defined according to the literature [27]. At the air inlet selection the constant mass flow of 0.8 kg/s and constant temperature of 650 K is prescribed, the fuel inlet is defined with the constant mass flow of 0.023 kg/s, and constant temperature of 300 K. At the outlet selection the static pressure was set up to 9.12 bar and the adiabatic boundary conditions was set for all wall selections. For mesh dependency tests all wall boundary conditions were defined with a constant temperature of 293.15 K, and fuel injection was not modelled. The used initial conditions are shown in Table 3. At the start of the simulation, the whole domain was initialized with the quiescent air, and the initial pressure was set to same value as defined on the outlet selection. The initial temperature is equal to the inlet temperature due to the assumption that this will be the minimum temperature inside the combustion chamber. The density of air was calculated from the ideal gas law, whilst the turbulent length scale and turbulent kinetic energy were selected as default values in AVL FIRE™ [17].

Table 3 Initial conditions

Pressure	9.12 bar
Temperature	650 K
Turbulent length scale	0.001 m
Turbulent kinetic energy	0.001 m^2s^{-2}
Density	Ideal gas

3.4. Spray setup

Schematic of fuel nozzle is shown in Figure 14. Particle size on fuel inlet is set to 150 μm. Three different simulations with different spray angle were performed. Spray angle is defined with two angle, δ_1 and δ_2, where δ_1 stands for half outer cone angle, and δ_2 for half inner cone angle. The difference between them defines the real spray angle. In Table 4 three different spray angle configurations are shown. The outer and inner diameter were held constant for all three different sprays. The liquid fuel used in performed simulations entitled as Jet-A is a surrogate for the kerosene fuel.

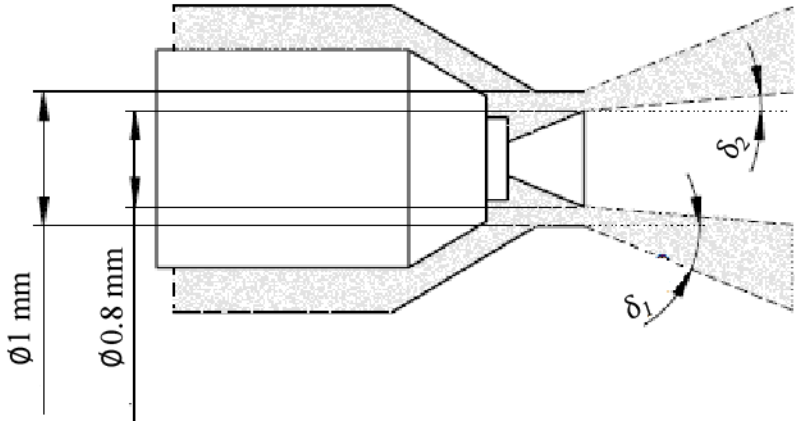

Figure 14 Schematic of fuel nozzle

Table 4 Spray angle

Spray angle [°]	$\boldsymbol{\delta_1}$ [°]	$\boldsymbol{\delta_2}$ [°]
15	18	3
20	22	2
25	28	3

3.5. Simulation setup

For turbulence and energy transport equations the first order Upwind Differencing Scheme (UDS) was applied, whilst for the continuity equation, the Central Differencing Scheme (CDS) was employed. For the momentum equation, a combination of CDS and UDS was proposed by introducing a blending factor of *0.5* [18][28]. The convergence of the solution was achieved when the normalised momentum and energy residuals reached a value lower than 10^{-4}, and pressure residual lower than $5 \cdot 10^{-4}$. The pressure-velocity coupling was performed by using the SIMPLE algorithm. The time discretization level was varied over simulation time based on the Courant-Friedrichs-Lewy (CFL) number of the gas phase [29]. At the beginning of the injection process, the time-step size was set to $1 \cdot 10^{-7} s$ and it was increased to a maximum value of $1 \cdot 10^{-5} s$.

4. RESULTS

This section shows the results of performed simulations where initially, the mesh dependency test results are discussed. Afterwards, the results, such as velocity, temperature and emission distribution through the combustion chamber, at the quasi- stationary state are shown.

4.1. Mesh dependency

Results which were observed are velocity and temperature distribution around the swirler for two different time frames and streamlines through the combustion chamber for three different computational meshes.

4.1.1. Mesh dependency results for time frame 1 ms

In Figure 15 the velocity and temperature fields around the swirler area, recorded at 1 ms are shown. At this time instance, the quasi stationary state around swirler is not reached yet. The velocity fields are similar for all three computational meshes, whilst for the temperature distribution, a small deviation between rough and finer meshes is noticed.

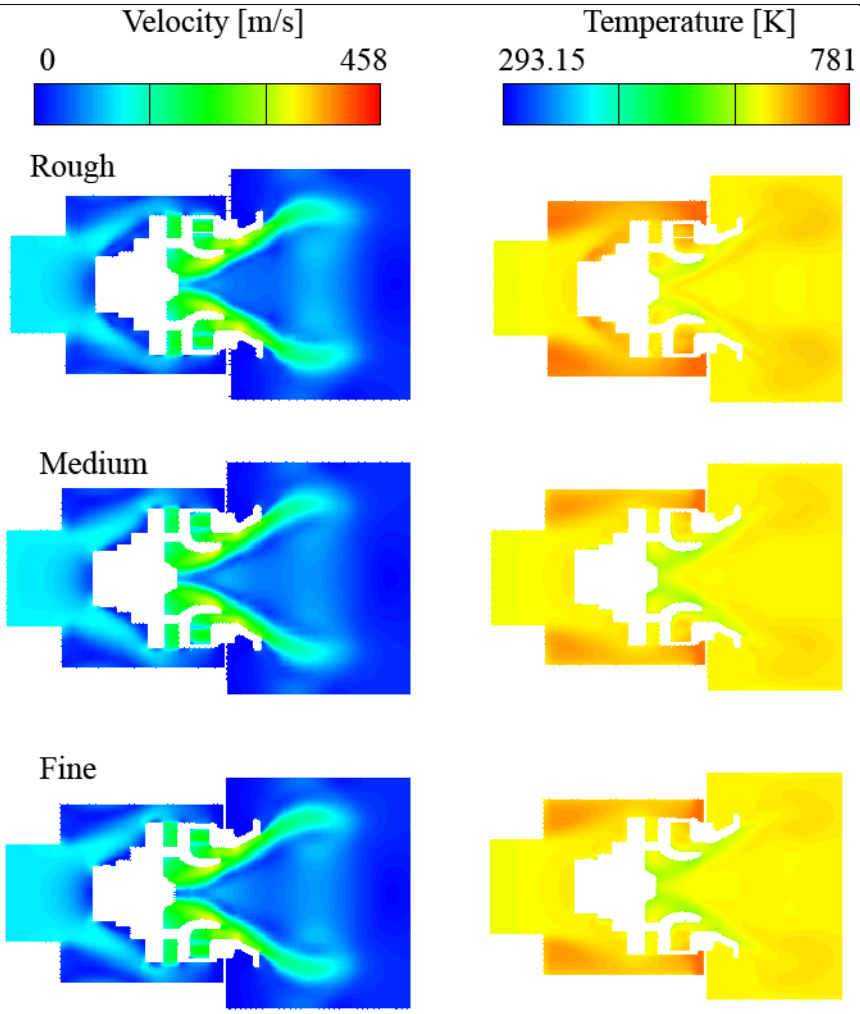

Figure 15 Velocity and temperature field at 1 ms

4.1.2. Mesh dependency results for time frame 2 ms

In Figure 16 the velocity and temperature distributions recorded at 2 ms are shown. At this time instance, the simulation reached quasi stationary state. The given results are matching for all three computational meshes, where a small deviation recorded in temperature distribution between rough and finer mesh is noticed. On the same figure, it can be seen that the air velocity increases through the swirler and additionally small vortices are generated.

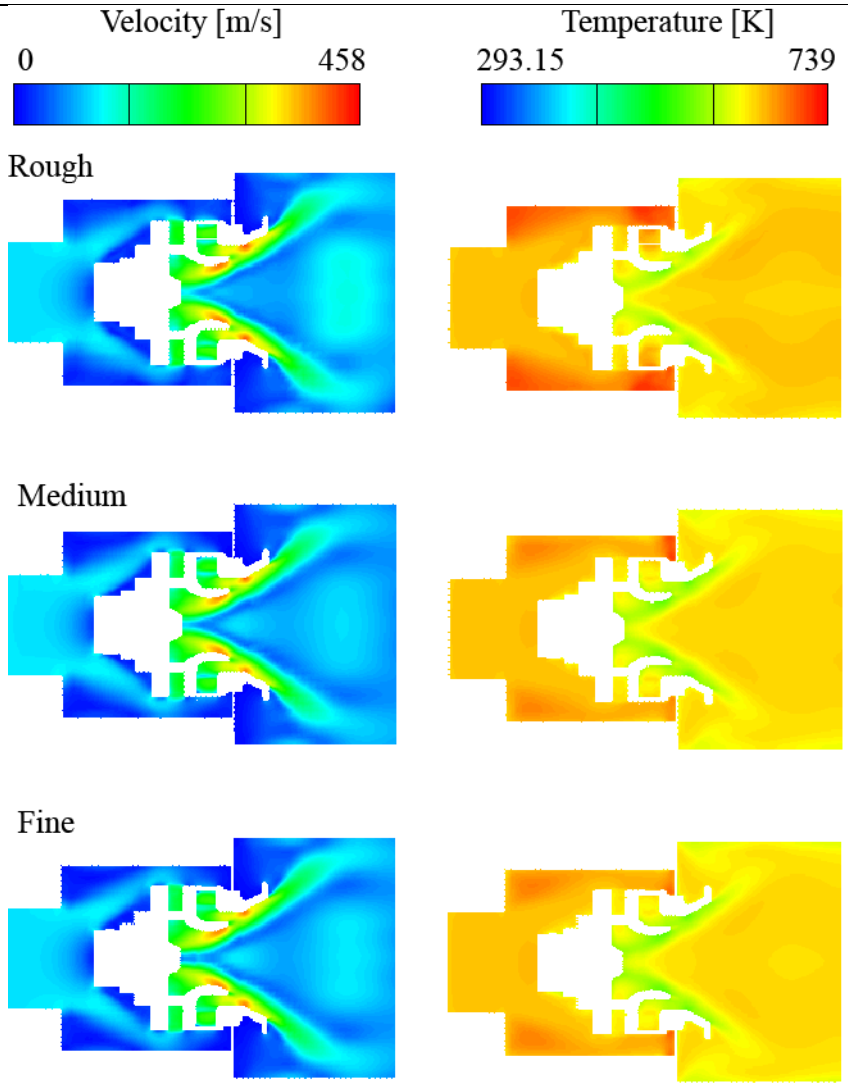

Figure 16 Velocity and temperature field at 2 ms

In Figure 17 the cross section, located at distance 0.1 m from the air inlet selection in the x-axis direction is shown. It can be noticed that the uniform airflow is generated after swirler for all three computational meshes.

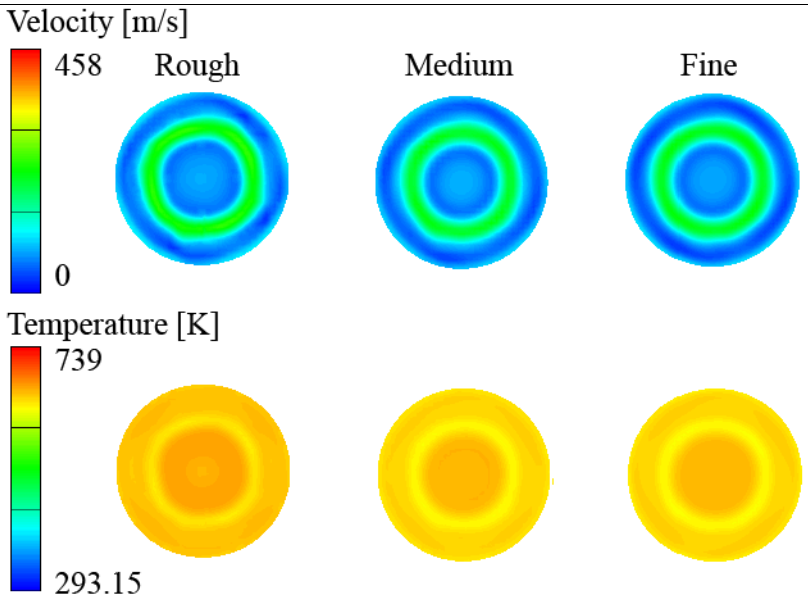

Figure 17 Velocity and temperature field in section in direction of *x* axis

In Figure 18 streamlines through the whole combustor are shown. Streamlines are colour mapped with velocity. As it was already stated, the velocity increases by passing through the swirler and the vortices are formed. Downstream from the swirler, at the same distance, streamlines form uniform flow for all three observed meshes.

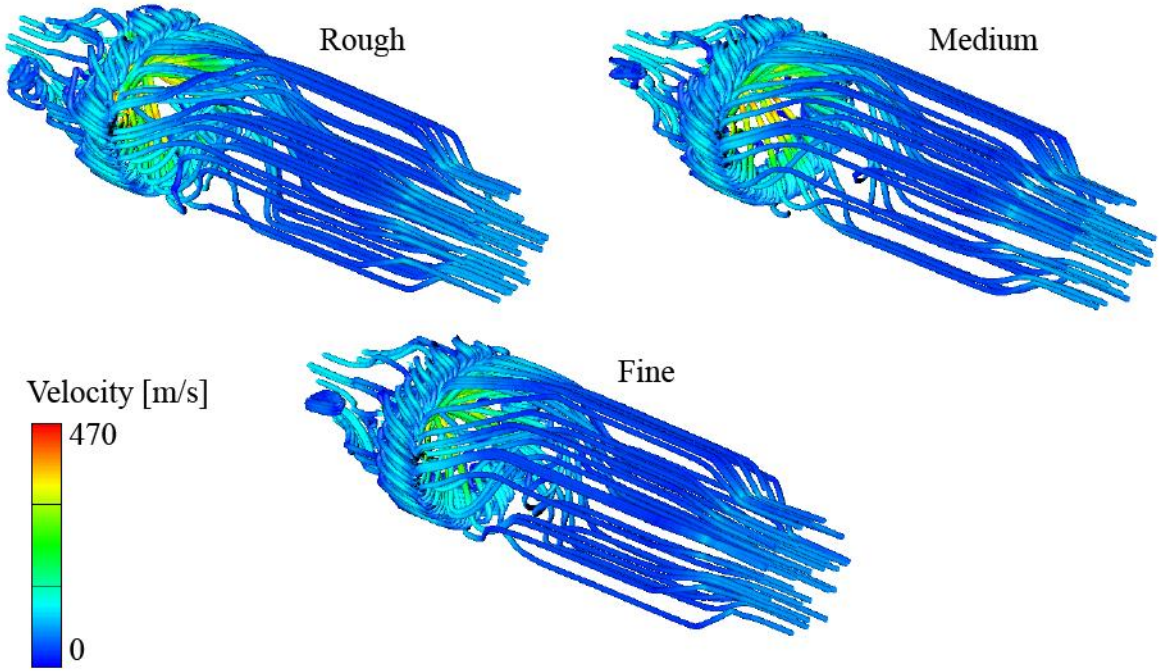

Figure 18 Streamlines through combustor

Mesh dependency tests shown that during air flow through the radial swirler, and after reaching the quasi stationary state, results are similar for all three observed computational meshes. Since only a small deviation in temperature and air flow direction between rough and finer mesh is noticeable, the rough mesh was used in further study. It is considered that the chosen mesh provides satisfying results for the purpose of this research.

4.2. Quasi stationary state

The quasi stationary state is determined when oscillations in mean temperature and NO_x mass fraction during simulation remain at low values. In Figure 19 it is shown that the mean temperature inside combustion chamber reaches quasi stationary state after $20\,ms$, and observing the NO_x mass fraction, the quasi stationary state is reached after $30\,ms$. These diagrams are shown for spray angle of $20°$, while for the simulations with other spray angle the quasi stationary state was achieved at similar simulation time period. Further results, referenced with the quasi stationary state are shown at the simulation time equal to $30\,ms$.

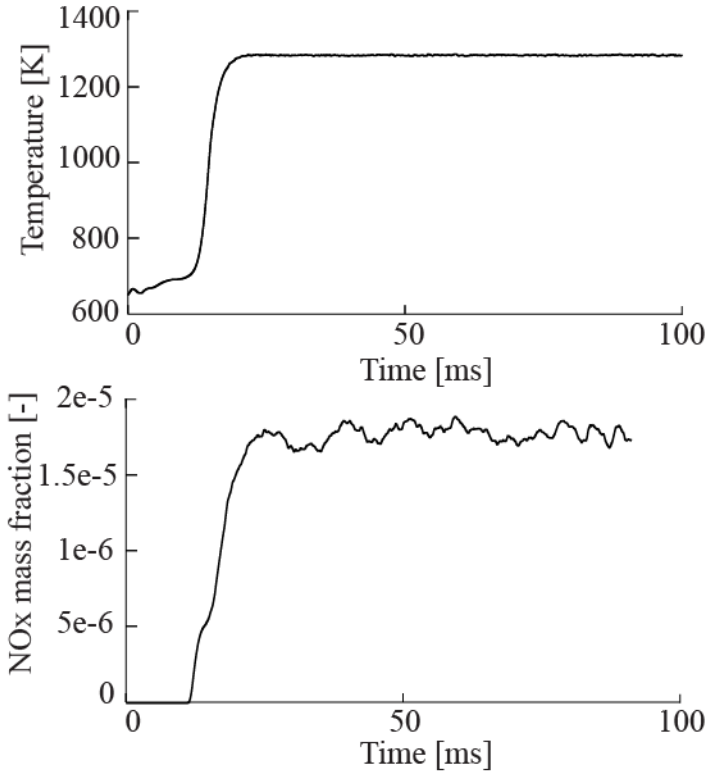

Figure 19 Mean temperature and NO_x mass fraction in the combustion chamber

4.3. Spray

The fuel injection starts at 2 ms of simulation. Three different simulations were performed with different spray angle. On left-hand side of Figure 20 the spray clouds for different spray angle simulation are shown. It is visible that with higher spray angle, the spray cloud is wider. On the right-hand side of Figure 20 the isosurface of evaporated fuel for different spray angle simulation are shown. It can be observed that for simulation with spray angle 15° and 20° the evaporated fuel exhibits similar shape, and with spray angle 25° less fuel is being evaporated.

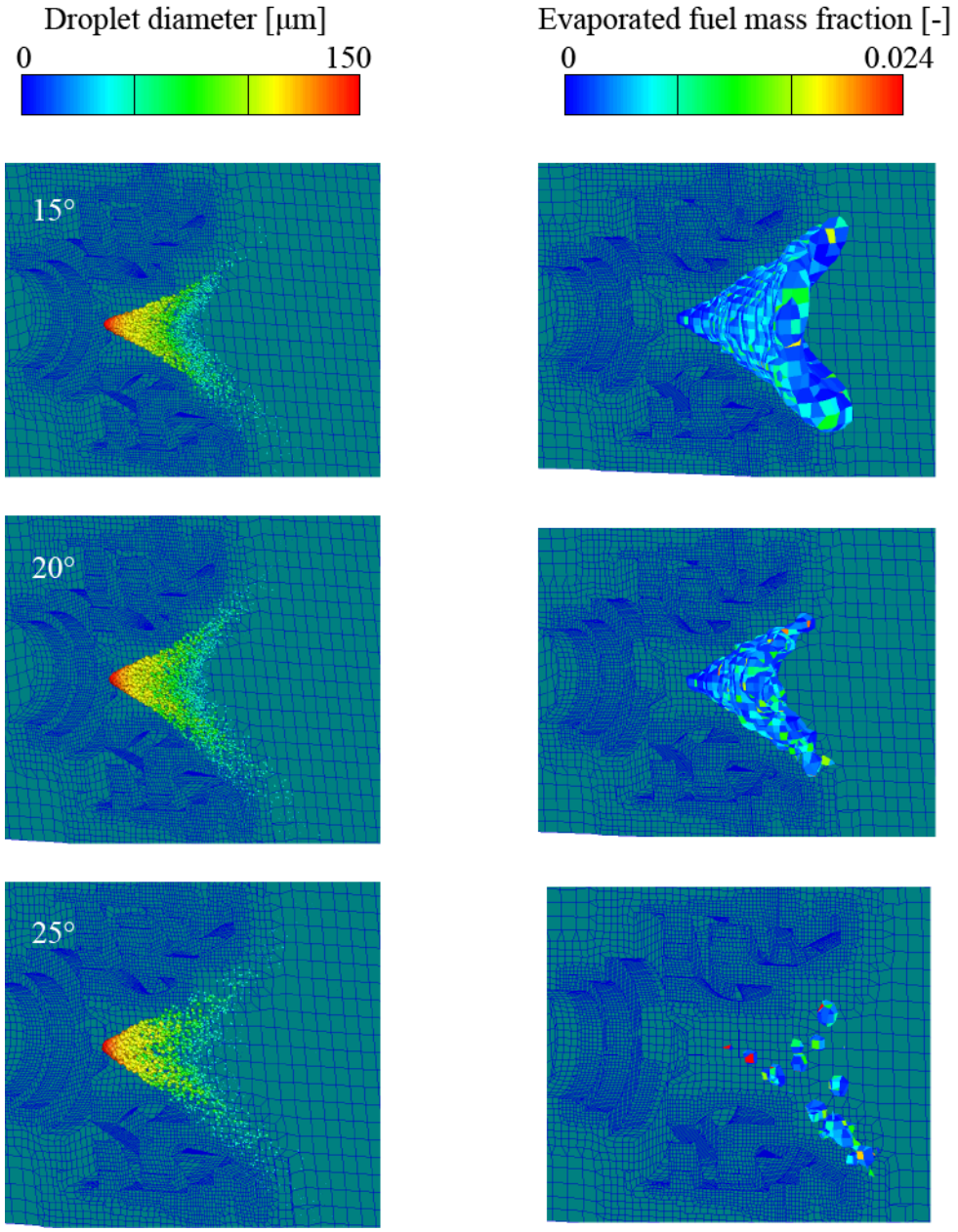

Figure 20 Spray cloud and isosurface of evaporated fuel for different spray angle

In Figure 21 the temperature distribution for different spray angle simulations is shown. It is visible that for spray angle of 15° and 20° the local temperature is much higher and more uniformly distributed through the combustion chamber, comparing to the simulation with spray angle 25°. Temperature with the spray angle of 20° is higher, comparing to simulation with spray angle 15°.

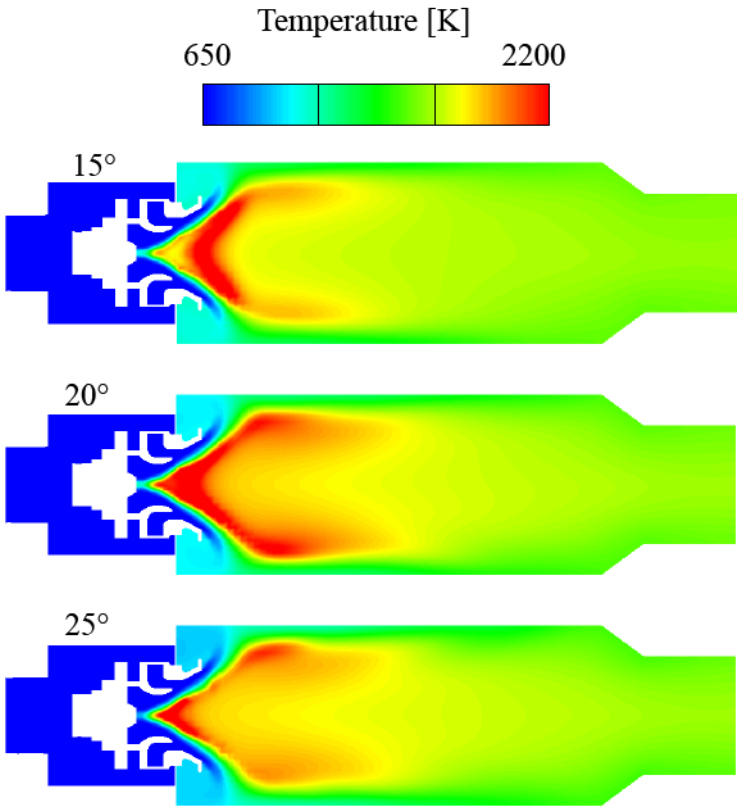

Figure 21 Temperature distribution for different spray angles

In Figure 22 the NO_x distribution for different spray angle is shown. The NO_x distributions are similar for simulations with spray angle 15° and 20° and it is much higher when comparing it to the simulation with spray angle defined with 25°.

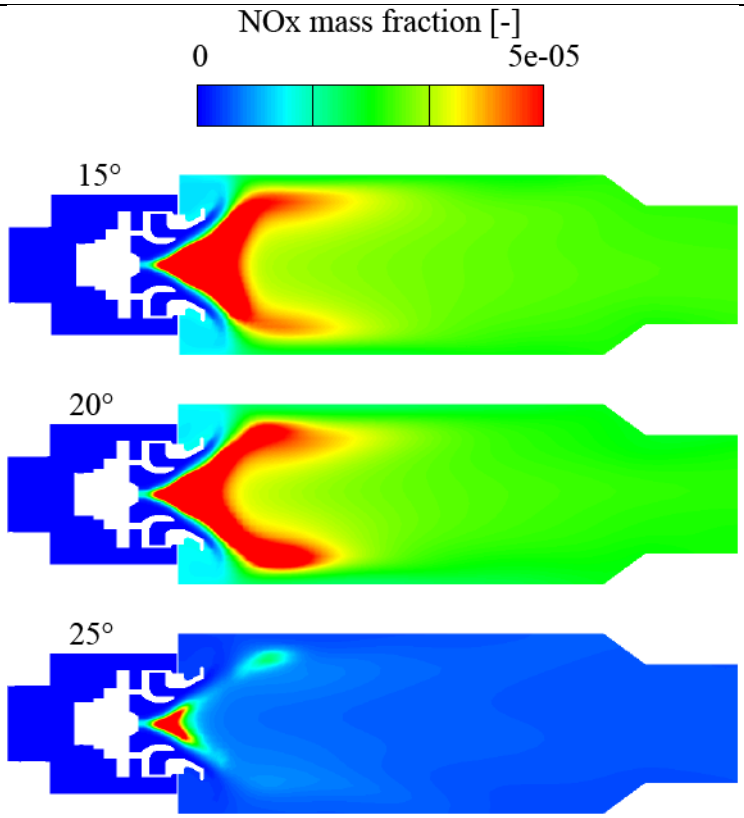

Figure 22 NOx distribution for different spray angles

Considering the results shown above, all other results will be shown for the simulation where spray angle was set to 20°.

The spray formation is shown in Figure 23. On the left-hand side of Figure 23**Error! Reference source not found.** fuel droplets colour mapped with their diameter are shown. The biggest droplets are in a range of 150 μm near the fuel inlet as it is prescribed in the spray setup, and they are getting smaller by the influence of the disintegration and evaporation processes. Eventually, they evaporate and the vapour cloud is formed. On the right-hand side of Figure 23 the droplets colour mapped with their velocity are shown. At the fuel inlet selection, the droplet velocity is in a range of 100 m/s and the velocity increases because of the influence of the accelerating air.

In Figure 24 the evaporated fuel is shown at the developed spray state. The isosurface of evaporated fuel represents the part of the combustion chamber where the evaporated fuel mass fraction is 0.005.

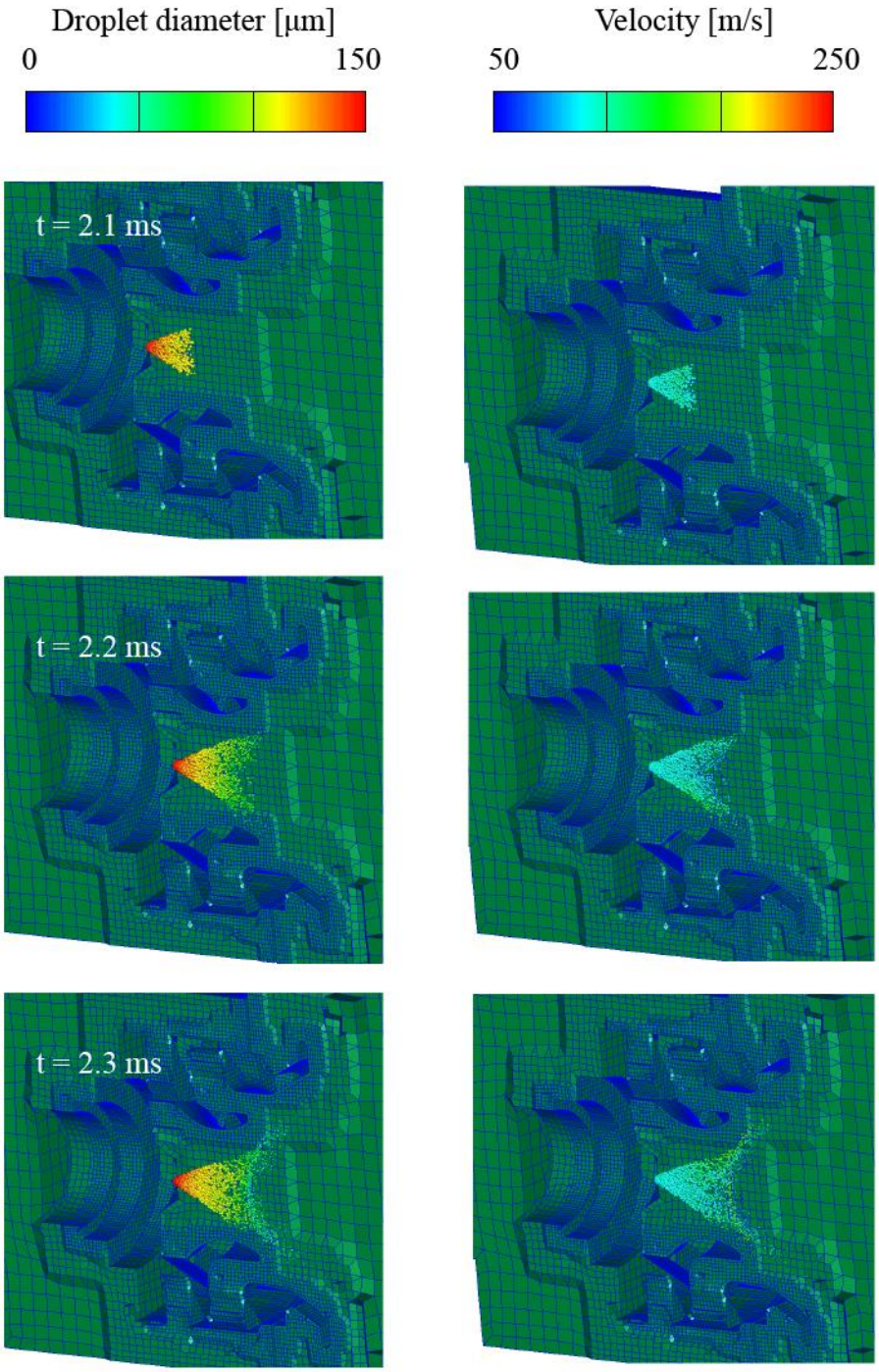

Figure 23 Spray formation with spray angle 20°

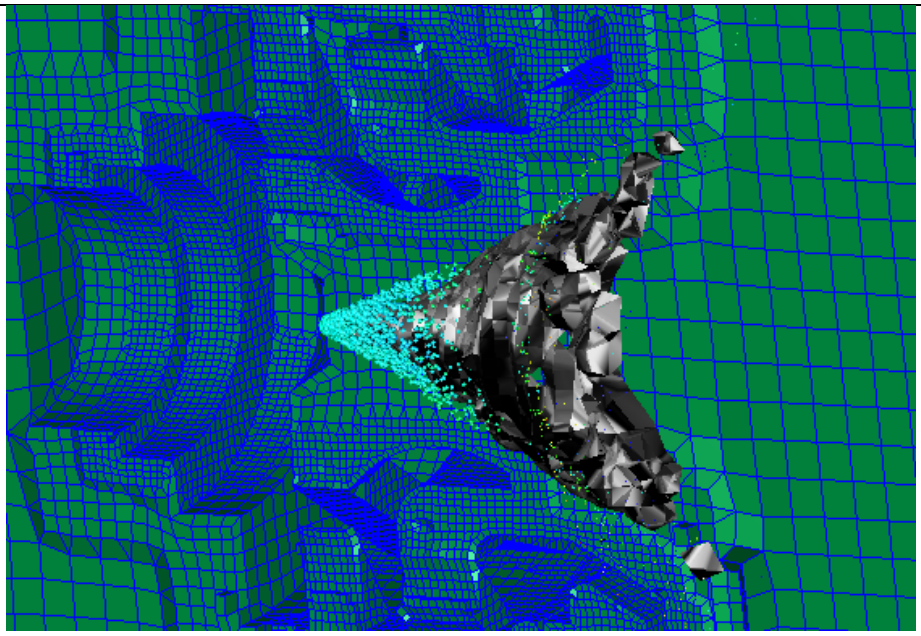

Figure 24 Isosurface of evaporated fuel with spray angle 20°

4.4. Combustion

As it is seen in Figure 25 the combustion process starts after approximately $15\,ms$ of simulation. The ignition process of fuel-air mixture is modelled with six spark plugs placed inside the combustion chamber. In this research, to speed up the convergence of simulation, multiple spark plugs were used. In Figure 25 the development of high temperature regions is shown. On the left-hand side, the temperature fields are shown for four different time instances, whilst on the right-hand side of the same figure, the formation of NO_x distribution is shown. It is visible that in the lower temperature regions the NO_x is not produced. When the temperature reaches higher values, the NO_x is created and the NO_x distribution follows the high temperature region.

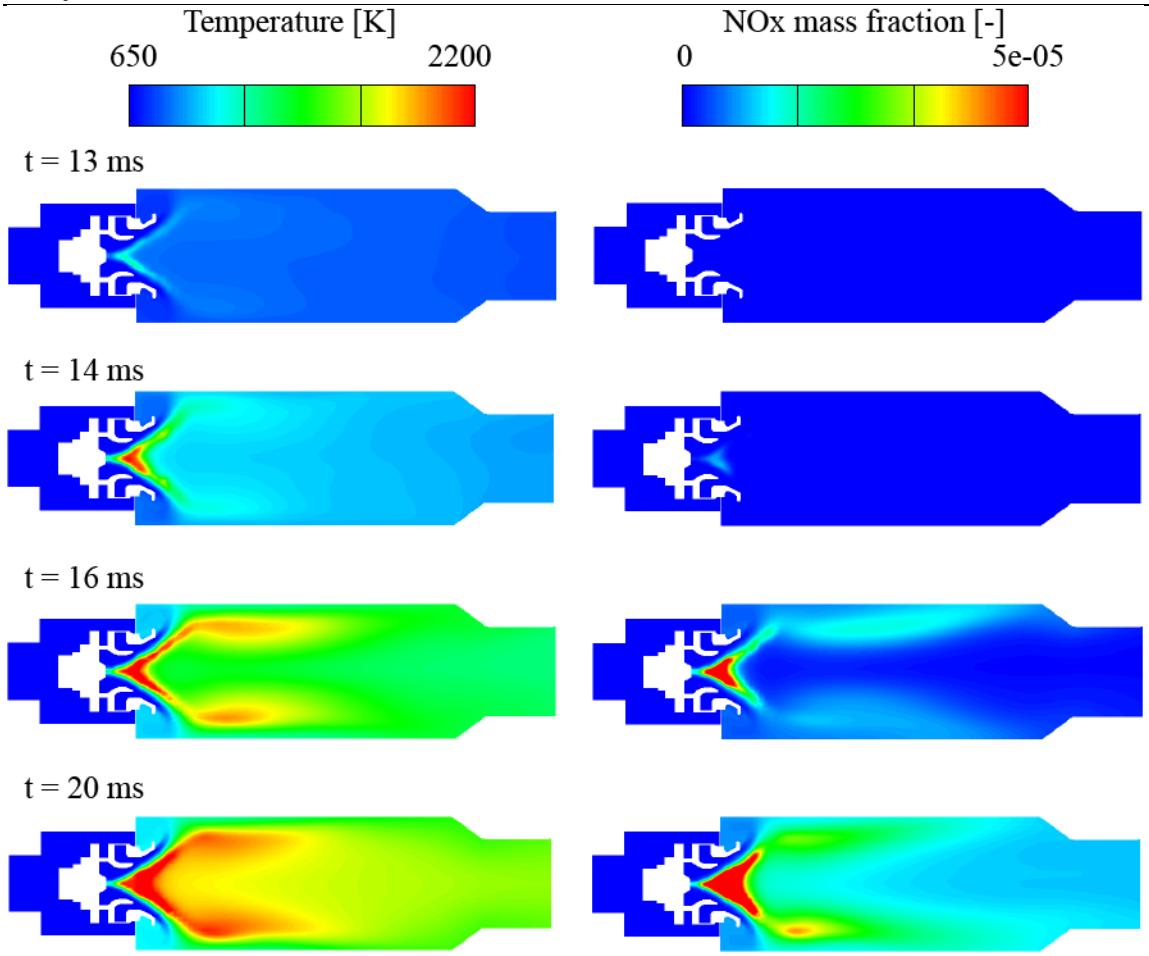

Figure 25 Temperature and NO_x distribution through combustion chamber

In Figure 26 the temperature and emission fields at quasi stationary state are shown. On the upper of Figure 26 the temperature field is shown. It is visible that the temperature is highest near the swirler and decreases towards the combustion chamber outlet. On the downside of Figure 26, the NO_x distribution at the quasi stationary state is shown. The highest NO_x mass fraction is noticed in the burning zone, and it decreases towards the outlet. The NO_x mass fraction is lower in the middle of the combustion chamber because the lack of oxygen which is consumed by the combustion process.

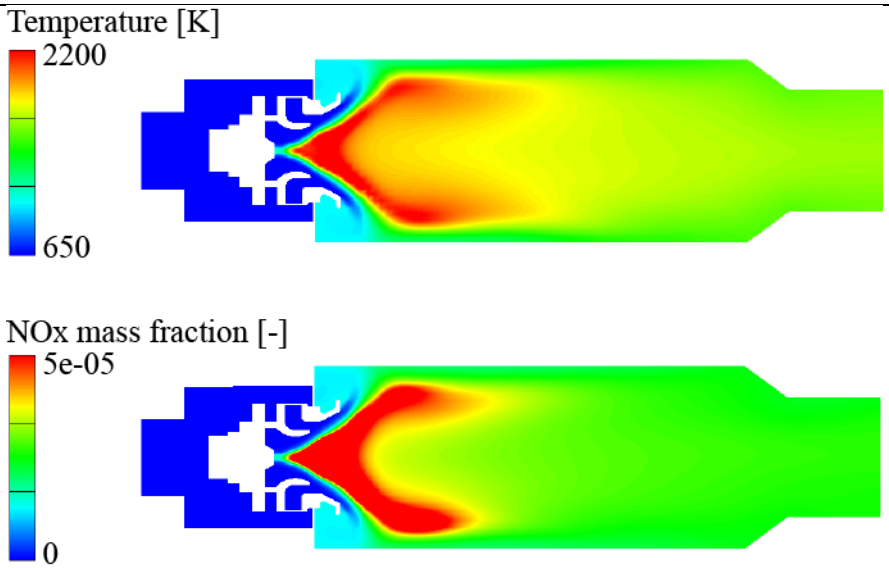

Figure 26 Temperature (up) and NOx (down) distribution at quasi stationary state

The temperature and NO_x mass fraction distributions for cross sections placed at different distances in the x-axis direction are shown in Figure 27. First section is located at $100\ mm$, and every following section is placed further downstream for $10\ mm$. From the given results it can be concluded that the uniformly smooth stream of heated gasses is reached, which is important to minimise pressure loss in the turbine section.

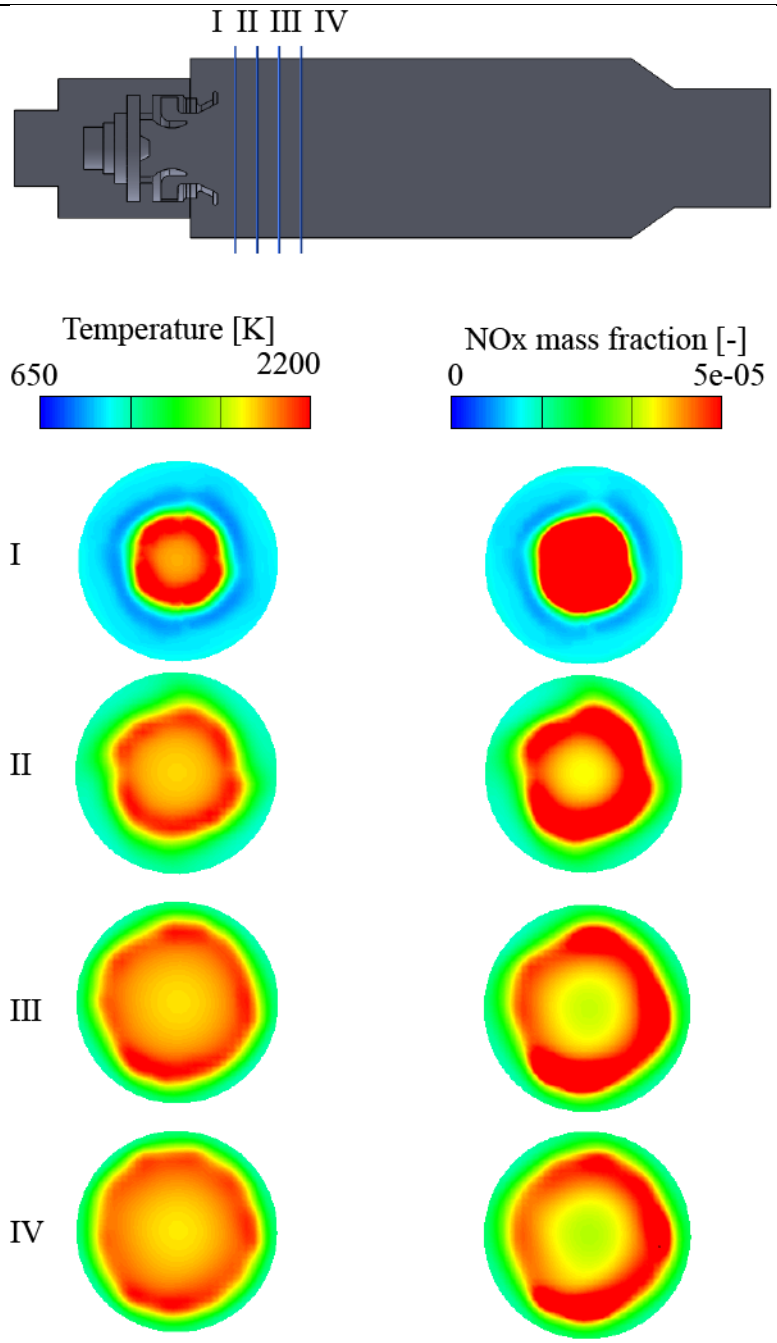

Figure 27 Temperature (left) and NO_x (right) distribution at different locations in the streamwise direction

5. CONCLUSION

Initially, the mesh dependency test was performed and conclusion which computational mesh provides optimal choice between solution accuracy and calculation time was determined. The presented results show that the rough mesh provides satisfying results for the purpose of this research. The quasi stationary state was determined when oscillation in mean temperature and NO_x mass fraction inside combustion chamber remain at a low value. It was determined that for all simulations such state was achieved after $30\ ms$ of simulation time. One objective of this research was to analyse the spray influence on combustion process. Spray influence on combustion process was analysed through three different simulations varying the spray angle. From shown results, it can be concluded that there is a significant influence of spray on combustion process in the observed combustion chamber. The highest temperature was reached with spray angle $20°$ and NO_x mass fraction was also highest within this spray angle, whilst the lowest temperature and NO_x mass fraction was reached with spray angle $25°$. The formation of spray cloud shape was analysed and the formation of high temperature region was shown. It was shown that the formation of NO_x inside the combustion chamber follows the temperature distribution. The highest temperature is noticed near the swirler area and it decreases towards the outlet selection. Results shown that inside of the observed combustion chamber, a uniformly smooth stream of heated gases is generated. Observing the provided results, it can be concluded that the correct chemical and physical behaviour of simulation setup was achieved. The given simulation setup could be implemented to a more complex jet engine combustion chamber.

LITERATURE

[1] Cox B. Turbines vs. Pistons 2012.

[2] Brayton cycle n.d. https://en.wikipedia.org/wiki/Brayton_cycle (accessed December 11, 2016).

[3] Rolls-Royce plc. The Jet engine, fifth edition. 1986.

[4] Mikulčić H, von Berg E, Vujanović M, Priesching P, Perković L, Tatschl R, et al. Numerical modelling of calcination reaction mechanism for cement production. Chem Eng Sci 2012;69:607–15. doi:10.1016/j.ces.2011.11.024.

[5] Mikulčić H, Vujanović M, Duić N. Improving the sustainability of cement production by using numerical simulation of limestone thermal degradation and pulverized coal combustion in a cement calciner. J Clean Prod 2015;88:262–71. doi:10.1016/j.jclepro.2014.04.011.

[6] Petranović Z, Edelbauer W, Vujanović M, Duić N. Modelling of spray and combustion processes by using the Eulerian multiphase approach and detailed chemical kinetics. Fuel 2017;191:25–35. doi:10.1016/j.fuel.2016.11.051.

[7] Xia H, Tucker PG, Dawes WN. Level sets for CFD in aerospace engineering. Prog Aerosp Sci 2010;46:274–83. doi:10.1016/j.paerosci.2010.03.001.

[8] Petranović Z. Numerical modelling of spray and combustion processes using the euler eulerian multiphase approach, University of Zagreb 2016.

[9] Chrigui M, Moesl K, Ahmadi W, Sadiki A, Janicka J. Partially premixed prevalorized kerosene spray combustion in turbulent flow. Exp Therm Fluid Sci 2010;34:308–15. doi:10.1016/j.expthermflusci.2009.10.023.

[10] Zhang G, Hung DLS. Temporal investigations of transient fuel spray characteristics from a multi-hole injector using dimensionless analysis. Exp Therm Fluid Sci 2015;66:150–9. doi:10.1016/j.expthermflusci.2015.03.011.

[11] Yu W, Yang W, Tay K, Mohan B, Zhao F, Zhang Y. Macroscopic spray characteristics of kerosene and diesel based on two different piezoelectric and solenoid injectors. Exp Therm Fluid Sci 2016;76:12–23. doi:10.1016/j.expthermflusci.2016.03.008.

[12] Orain M, Hardalupas Y. Droplet characteristics and local equivalence ratio of reacting mixture in spray counterflow flames. Exp Therm Fluid Sci 2014;57:261–74. doi:10.1016/j.expthermflusci.2014.05.009.

[13] Sommerfeld M, Berend van Wachem. Best Practice Guidelines for Computational Fluid Dynamics of Dispersed Multiphase Flows. vol. 8. 2008.

[14] AVL FIRE Documentation, Combustion module, v2014_1 2014.

[15] Hanjalić K, Popovac M, Hadžiabdić M. A robust near-wall elliptic-relaxation eddy-viscosity turbulence model for CFD. Int J Heat Fluid Flow 2004;25:1047–51. doi:10.1016/j.ijheatfluidflow.2004.07.005.

[16] Durbin, P A. Near-wall turbulence closure modeling without "damping functions" 1991.

[17] AVL Fire Documentation, v2014_01 2014.

[18] FIRE Manual 2013: Graz 2013.

[19] Petranović Z, Vujanović M, Duić N. Towards a more sustainable transport sector by numerically simulating fuel spray and pollutant formation in diesel engines. J Clean Prod 2015;88:272–9. doi:10.1016/j.jclepro.2014.09.004.

[20] Brenn, Günter, Deviprasath, L.J. and Durst F. Computations and Experiments on the Evaporation of Multi-Component Droplets, Proc.9th Int.Conf.Liquid Atomiz.Spray Syst. (ICLASS), Sorrento (Italy) 2003.

[21] Abramzon B, Sirignano WA. Droplet vaporization model for spray combustion calculations. Int J Heat Mass Transf 1989;32:1605–18. doi:10.1016/0017-9310(89)90043-4.

[22] Colin O, Benkenida A. The 3-Zones Extended Coherent Flame Model (ECFM3Z) for Computing Premixed/Diffusion Combustion. Oil Gas Sci Technol – Rev IFP 2004;59:593–609.

[23] Vujanović M. Numerical Modelling of Multiphase Flow in Combustion of Liquid Fuel. University of Zagreb, 2010.

[24] Duić N. Prilog matematičkom modeliranju izgaranja plinovitog goriva u ložištu generatora pare. University of Zagreb, 1998.

[25] Fenimore CP. Formation of nitric oxide in premixed hydrocarbon flames. Symp Combust 1971;13:373–80. doi:10.1016/S0082-0784(71)80040-1.

[26] 3D CAD Design Software | SOLIDWORKS n.d. http://www.solidworks.com/ (accessed June 6, 2017).

[27] Hajivand M. Cfd Modeling of Kerosene Combustion With Various Initial Conditions and Fuel Droplet Diameters 2015;16.

[28] Petranović Z, Vujanović M, Duić N. Numerical modelling of diesel spray using the Eulerian multiphase approach. J Clean Prod 2015;88:272–9. doi:10.1016/j.jclepro.2014.09.004.

[29] Courant–Friedrichs–Lewy condition n.d. https://www.cfd-online.com/Wiki/Courant–Friedrichs–Lewy_condition (accessed March 8, 2017).

ATTACHMENTS

I. CD-R disc